

Ocean circulation and exchanges through the northern Bering Sea—1979–2001 model results

J.L. Clement^{a,*}, W. Maslowski^a, L.W. Cooper^b, J.M. Grebmeier^b, W. Walczowski^c

^a*Department of Oceanography, Naval Postgraduate School, Monterey, CA, USA*

^b*Department of Ecology and Evolutionary Biology, University of Tennessee, Knoxville, TN, USA*

^c*Institute of Oceanology, Polish Academy of Sciences, Sopot, Poland*

Received 1 July 2004; accepted 12 September 2005

Abstract

We have developed and run a model with sufficiently high resolution (~9 km and 45 levels) and a large enough spatial domain to allow for realistic representation of flow through the narrow and shallow straits in the northern Bering Sea. This is potentially important for quantification of long-term mean and time-dependent ocean circulation, and water mass and property exchanges between the Pacific and Arctic Oceans. Over a 23 year interval (1979–2001), mean transport through Bering Strait is estimated to be 0.65 Sv. Comparison of our model results with published observations indicates that ocean circulation is not only variable at seasonal to interdecadal scales but it is also responsive to short-term atmospheric forcing. One of such events occurred during the winter of 2000–2001 with reversed oceanic flow in some areas and much reduced sea-ice cover. Analyses of eddy kinetic energy fields identify some high biological productivity regions of the Chirikov Basin coincident with persistent high energy (up to $2700 \text{ cm}^2 \text{ s}^{-2}$ in the surface layer and up to $2600 \text{ cm}^2 \text{ s}^{-2}$ at mid-depth) throughout the annual cycle. Model output in the Bering Strait region is validated against several time series of moored observations of water mass properties. Comparison with shipboard observations of near-bottom salinity from late winter through autumn indicates that the model reasonably represents the major water-mass properties in the region. The modeled vertical water-column structure in the northern Bering Sea allows increased understanding of the mechanisms of water transformation and transport northward through Bering Strait into the Chukchi and Beaufort Seas. We conclude that the long-term model results for the northern Bering Sea provide important insights into the ocean circulation and fluxes and they are a useful frame of reference for limited observations that are short-term and/or cover only a small geographic region.

Published by Elsevier Ltd.

Keywords: Bering Sea; Polar oceanography; Numerical models; Ocean circulation

1. Introduction

Estimation of flow through Bering Strait presents several challenges to both observational and model-

ing studies. This narrow (85 km wide) strait is the only communication passage between the Pacific and Arctic Oceans. The political boundary between the U.S. and Russia divides the strait and restricts access to potential investigators. Ice floes with deep drafts are a threat to moorings placed in the upper 40 m of the strait (Roach et al., 1995). Due to substantial horizontal shear, extrapolation of

*Corresponding author. Tel.: +1 831 656 3226;
fax: +1 831 656 2712.

E-mail address: jlcllemen@nps.edu (J.L. Clement).

velocity measurements from one point to total transport is of uncertain validity, although the use of multiple current meters and regression techniques increases confidence in transport estimates (Aagaard et al., 1985). While political boundaries and ice draft do not significantly impede modeling efforts, the geomorphology (i.e. width and depth) of the strait and a large ocean to the north and south are challenging as they require a combination of high resolution and large domain to realistically represent the time-dependent and highly variable flow.

Currently, many global ocean circulation models either have a closed Bering Strait or instead use some type of prescribed conditions. Goosse et al. (1997) found that their treatment of a closed versus open Bering Strait had a significant impact on model results. Specifically, with an open Bering Strait their modeled oceanic and sea-ice transports through Fram Strait increased to more realistic values. Also the sea-ice edge in the Bering Sea was more realistically positioned further north due to warmer water advection across the Bering Sea. In addition, the modeled freshwater budget of the Greenland and Norwegian Seas and of the Atlantic Ocean was enhanced by the Bering Strait throughflow. Although general circulation models (GCMs) may not have high enough resolution to explicitly represent the exchanges through Bering Strait, results presented here indicate that such models can benefit from high-resolution regional modeling that can realistically account for flow through narrow straits. Improved understanding of ocean circulation and sea-ice conditions in data-limited regions should facilitate more realistic simulations in GCMs. This goal was central to our study, but in addition, we expected that results in the Bering Strait region would provide insight into the mean state and variability of water mass and property fluxes, such as heat and freshwater, into the Arctic Ocean. Upstream (southward) from Bering Strait, field observations have shown an east–west increase in salinity and nutrient concentrations (Walsh et al., 1989; Grebmeier and Cooper, 1995). In the west, deeper Pacific Water is generally upwelled onto the shelf within the Gulf of Anadyr, with relatively high salinity and nutrient content (Anadyr Water). A less saline and nutrient-rich water mass (Bering Shelf Water) is found in the central region of the northern Bering Sea, while a strong gradient defines the warmer (in summer), nutrient-poor Alaska Coastal Water to the east (Coachman, 1987; Grebmeier et al., 1988).

A limited number of modeling studies have concentrated on the northern Bering Sea (e.g., Overland and Roach, 1987; Spaulding et al., 1987; Nihoul et al., 1993). These studies have proven useful in simulating the major circulation features of the region. However, they have been limited by low spatial resolution and small domains with lateral boundary conditions prescribed in close proximity to the region of interest. In addition, these studies were integrated only for a short period of time (1–3 months). Recent advancements in computing capability and updated bathymetry information have allowed us to develop a relatively high-resolution (~9 km and 45 levels), large domain model encompassing the Bering Sea, which has been spun-up for 48 years and integrated with realistic interannual forcing for an additional 23 years.

The overarching goal of this research is to quantify the long-term mean and variability of the circulation and water-mass properties over short (monthly) to long (decadal) time scales across the data-limited northern Bering Sea and through Bering Strait using this pan-Arctic coupled ice-ocean model. One of our specific objectives in this study was to improve understanding of the flow and transports through Anadyr, Shpanberg, and Bering Straits (locations shown in Fig. 1). Model results are validated against observational data including salinity and nutrient concentrations in the Bering Sea, in addition to salinity and temperature measurements and volume transport estimates in Bering Strait.

2. Model description

The coupled sea-ice–ocean model has a horizontal grid spacing of $1/12^\circ$ (or ~9 km) and 45 vertical depth layers with eight levels in the upper 50 m. The high vertical resolution, especially in the upper water column, allows for more realistic representation of the shallow Arctic and sub-Arctic shelves as compared to previous models, which were only 2-dimensional (e.g., Overland and Roach, 1987; Spaulding et al., 1987). In addition, the horizontal grid permits calculation of flow through the narrow straits of the northern Bering Sea. The model domain contains the sub-Arctic North Pacific (including the Sea of Japan and the Sea of Okhotsk) and North Atlantic Oceans, the Arctic Ocean, the Canadian Arctic Archipelago (CAA) and the Nordic Seas (see Fig. 1A of Maslowski et al., 2004 for model domain). The region of interest, the

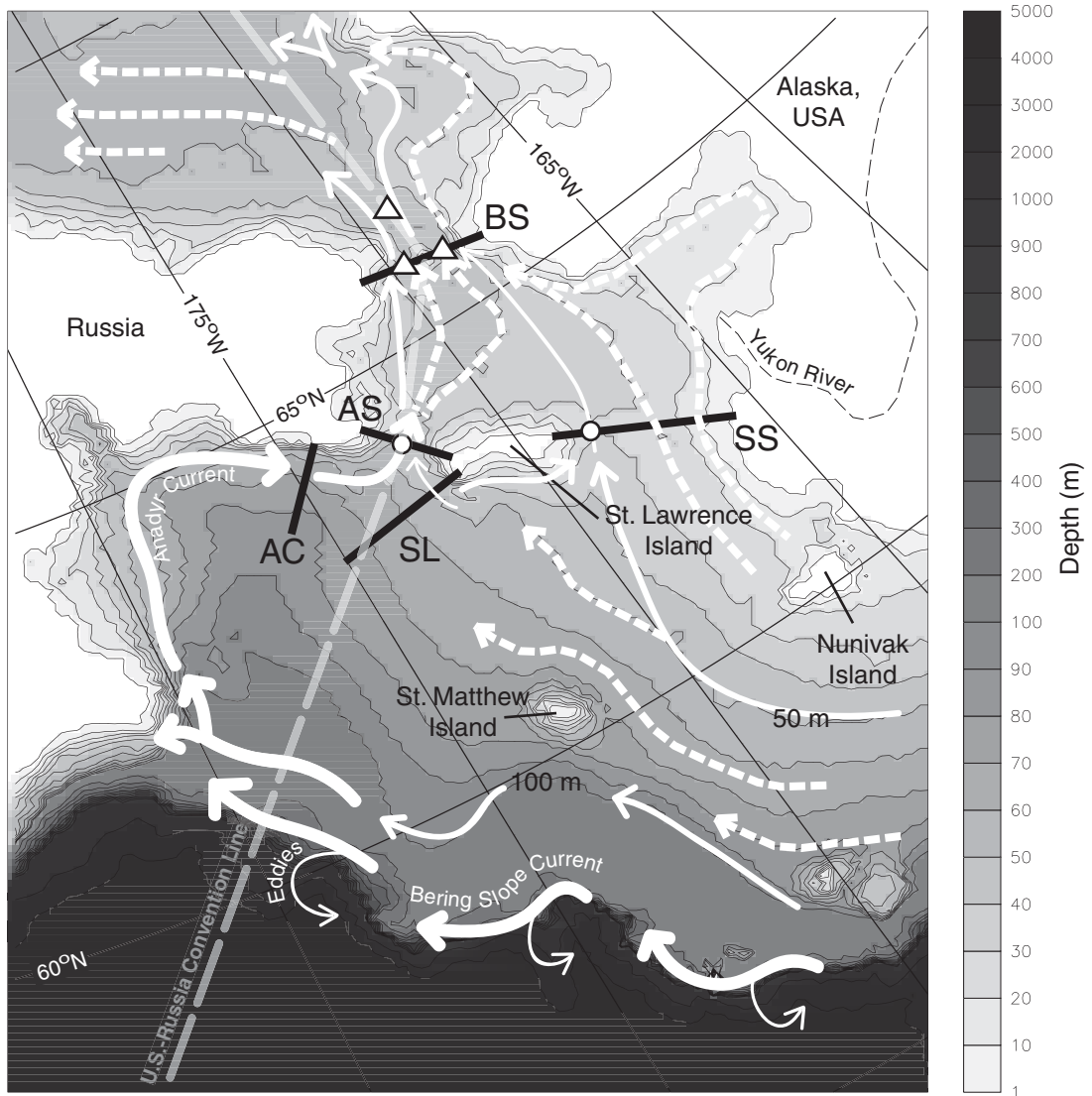


Fig. 1. Schematic of mean circulation in the Bering Sea adapted from Coachman (1993), Stabeno et al. (2001), and Hermann et al. (2002). Dashed arrows are proposed based on the results of this study. Thick black lines indicate model cross-sections: BS (Bering Strait), AS (Anadyr Strait), SS (Shpanberg Strait), AC (Anadyr Current), and SL (St. Lawrence Island). White circles indicate model stations in the deepest part of Anadyr Strait and Shpanberg Strait. White triangle indicate the locations of moorings and coincident model stations in the Eastern and Western channels of Bering Strait and at a North Central location. The U.S.-Russia Convention Line is indicated by a gray dashed line.

Bering Sea, is therefore far away from the artificially closed lateral boundaries in the North Pacific at $\sim 30^\circ\text{N}$, greatly reducing the potential effect of boundary conditions. Model bathymetry is derived from two sources: ETOPO5 at 5 km resolution for the region south of 64°N and International Bathymetric Chart of the Arctic Ocean (IBCAO; Jakobsson et al., 2000) at 2.5 km resolution for the region north of 64°N . The ocean model was initialized with climatological, 3-dimensional temperature and salinity fields (PHC; Steele et al., 2000) and integrated for 48 years in a spinup mode. During the spinup we initially used daily averaged annual climatological atmospheric forcing derived from 1979 to 1993 reanalysis from the European Centre for Medium-Range Weather Forecasts (ECMWF) for 27 years. We then performed an additional run using repeated 1979 ECMWF annual cycle for six years and then 1979–1981 interannual fields for the last 15 years of spinup. This approach is especially

nity fields (PHC; Steele et al., 2000) and integrated for 48 years in a spinup mode. During the spinup we initially used daily averaged annual climatological atmospheric forcing derived from 1979 to 1993 reanalysis from the European Centre for Medium-Range Weather Forecasts (ECMWF) for 27 years. We then performed an additional run using repeated 1979 ECMWF annual cycle for six years and then 1979–1981 interannual fields for the last 15 years of spinup. This approach is especially

important in establishing realistic ocean circulation representative of the time period at the beginning of the actual interannual integration. This final run with realistic daily averaged ECMWF interannual forcing starts in 1979 and continues through 2001. Results from this integration (23 years) are used for the analyses in this paper. Yukon (and other Arctic) river runoff is included in the model as a virtual freshwater flux at the river mouth. However, in the Gulf of Alaska the freshwater flux from runoff (Royer, 1981) is introduced by restoring the surface ocean level (of 5 m) to climatological (Polar Science Center Hydrographic Climatology; PHC) monthly mean temperature and salinity values over a monthly time scale (as a correction term to the explicitly calculated fluxes between the ocean and overlying atmosphere or sea-ice). Additional details on the model including sea-ice, river runoff, and restoring have been provided elsewhere (Maslowski et al., 2004).

3. Bering Sea circulation

Flow is generally northward in the Bering Sea throughout the year (Fig. 1) and intensification occurs in narrow straits such as Bering, Anadyr, and Shpanberg, as well as along the slope (Bering Slope Current (BSC)) and western boundary (Anadyr Current). The 23-year (1979–2001) modeled mean circulation in the upper 50 m (Fig. 2) is generally in agreement with previous studies such as Schumacher et al. (1983). In this study that we use as an example, a current meter mooring (64°N , 171.9°W) showed strong Anadyr Strait flow ($\sim 0.156\text{ m s}^{-1}$) directed northeastward toward the Chirikov Basin during November 1980 through June 1981. At another mooring located 40 km south of St. Lawrence Island (63°N , 171°W) flow was eastward at $\sim 0.036\text{ m s}^{-1}$, while only $\sim 0.005\text{ m s}^{-1}$ was recorded 60 km to the southwest of the island (63.1°N , 173.1°W). As in the Schumacher et al. (1983) dataset, in the model (Fig. 2), there is high northeastward velocity in Anadyr Strait, lower velocity directed eastward south of St. Lawrence Island and sluggish flow to the southwest of the island (note the color shading in Fig. 2). There is close agreement between model and data on these key features, although the model output also shows stronger flow along some isobaths (e.g., along the 50-m isobath and between the 60- and 70-m isobaths) across the central and eastern shelf south of St. Lawrence Island. Unfortunately, very few

published observational data are available to confirm these modeled features. The model represents the circulation in the Chirikov Basin (north of St. Lawrence Island) as a sweeping cyclonic flow bathymetrically steered toward Bering Strait, instead of a coastal jet moving straight to the western edge of Bering Strait, as depicted in Hermann et al. (2002). While it is possible that there is a narrow coastal jet, which may not be fully resolved using a 9-km grid cell, it seems likely that cold and salty Anadyr Water moving through Anadyr Strait (as represented in Fig. 9) would follow the local bathymetry into the deeper central portion of the Chirikov Basin.

Circulation varies seasonally (model output not shown) with higher velocities during spring and summer in the northern Bering Sea (NBS; defined as north of 62°N , south of 67°N and between 165°W and 175°W). Model output shows lower velocities during winter, especially under the sea-ice cover, although the middle shelf (south of the NBS and less than 500 m deep) actually intensifies during autumn and winter possibly in relation to ice-edge dynamics. It is also worth noting that just south of St. Lawrence Island eastward flow becomes more organized and stronger during spring and summer (not shown), which is not as apparent in the 23-year mean.

Interannual variation in the Bering Sea circulation is examined by comparing the year of highest modeled volume transport through Bering Strait (1979) with the year of lowest modeled transport (1994) (as shown in Fig. 5). The mean velocity in the upper 50 m of the region shown in Fig. 3A during 1979 is 0.044 m s^{-1} (Fig. 3A), while in 1994 it is only 0.033 m s^{-1} (Fig. 3B). A notable difference is much less organized flow in the east and the weaker flow in the central Bering Sea during 1994 compared to 1979. The difference in vector fields for 1979–1994 (Fig. 3C) also indicates significantly weaker flow during 1994 in the northern and eastern regions, as well as along the BSC. Differences along the BSC are likely due to variation in eddy activity. Across the region the mean difference between the two years is 0.025 m s^{-1} or $\sim 70\%$ of the 23-year mean (Table 1). We attribute these differences in flow to differences in wind speed and direction. Annually averaged wind fields (not shown) for 1979 and 1994 show much stronger wind ($2\text{--}3\text{ m s}^{-1}$) out of the north in the vicinity of Bering Strait during the year of lowest transport (1994). The stronger northerly winds appear to impede northward

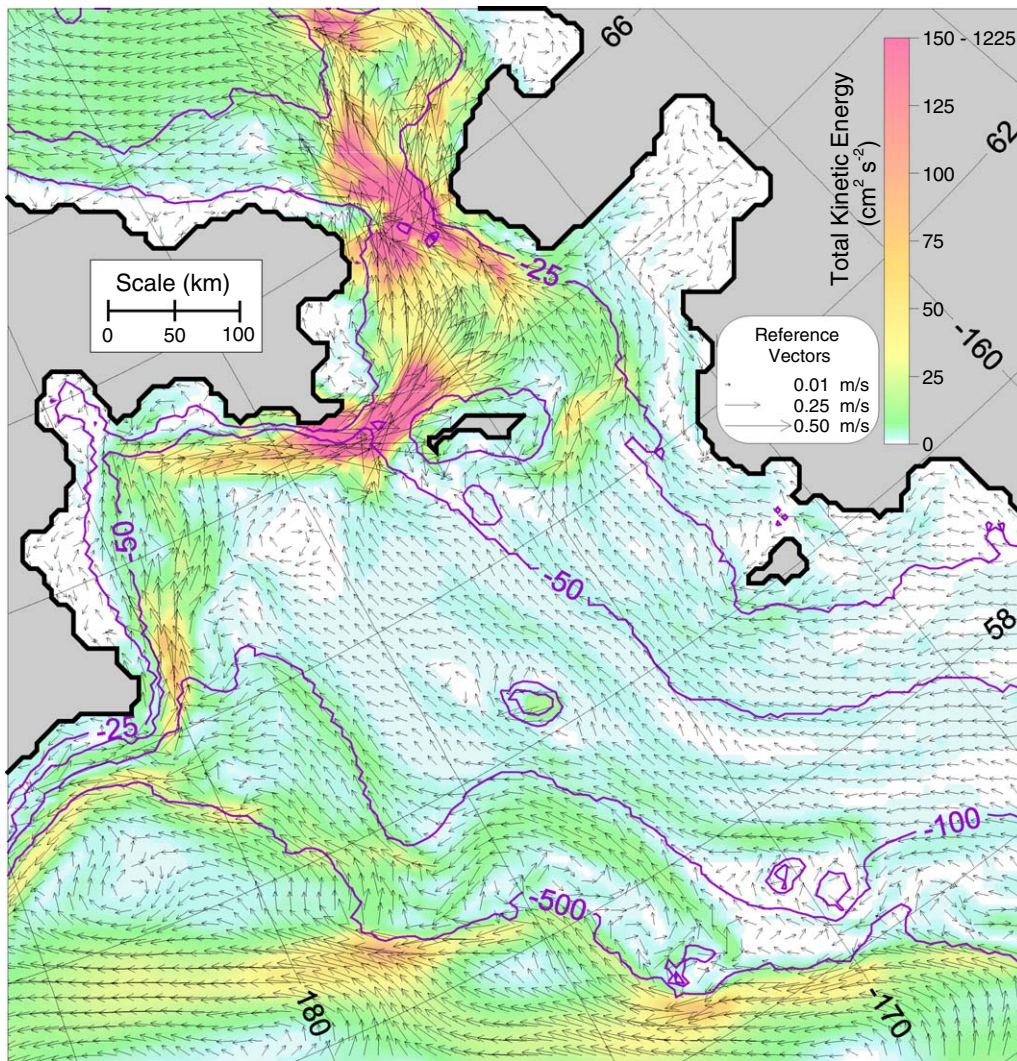


Fig. 2. Twenty-three-year mean velocity averaged over the upper 50 m. Twenty-five percent of vectors are shown. Color shading represents the total kinetic energy ($\text{cm}^2 \text{s}^{-2}$) calculated as $0.5 \cdot (u^2 + v^2)$.

oceanic transport through the strait and upstream. A different situation occurs in 1979 with weaker winds ($1.5\text{--}2 \text{ m s}^{-1}$) out of the northeast, which have less of an influence on northward transport.

4. Volume, freshwater, and heat transports

Five vertical cross-sections shown in Fig. 1 are analyzed for volume, freshwater, and heat transport in this section and compared to the limited observational data that are available. Based on data collected during 1990–1994, Roach et al. (1995) estimate the mean northward volume transport through Bering Strait to be 0.83 Sv (maximum error

of 30% or $\pm 0.25 \text{ Sv}$, $1 \text{ Sv} = 10^6 \text{ m}^3 \text{ s}^{-1}$). The modeled mean northward transport during the same time is 0.58 Sv with a standard deviation of $\pm 0.21 \text{ Sv}$, which is in the lower range of the observational estimate. The mean of the entire integration (1979–2001) is 0.65 Sv with a standard deviation of $\pm 0.23 \text{ Sv}$ (Table 2). Bering Strait (BS) and Anadyr Strait (AS) have similar annual cycles, showing higher monthly mean transport in summer up to ~ 0.95 and 0.80 Sv , respectively (Fig. 4A). This is consistent with measurements made by Roach et al. (1995) in Bering Strait, who reported higher velocities in the spring and summer months with winter values about 25% lower. Shpanberg Strait

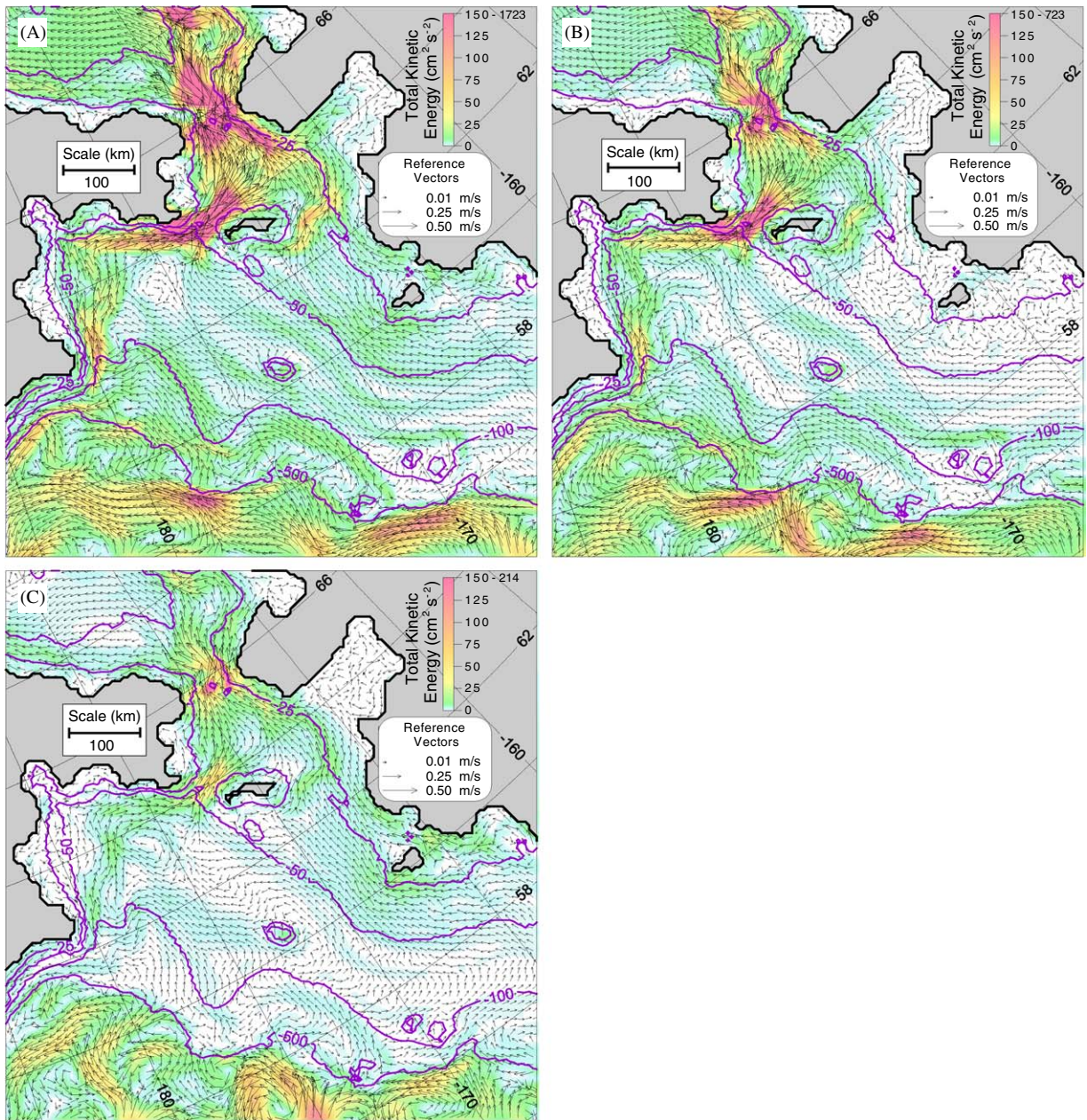


Fig. 3. Mean annual velocity in the upper 50 m during the year of (A) highest (1979) and (B) lowest (1994) northward transport through Bering Strait over the 23-year model integration and (C) the difference in the mean velocities of 1979 and 1994. Twenty-five percent of vectors are shown.

(SS) and Anadyr Current (AC) show relatively less variation over the annual cycle, with slightly higher transport in summer (Fig. 4A). Transport is generally northward across the St. Lawrence section (SL) except during February and March when the flow is reversed. This may be due to changes in wind forcing and density gradients caused by sea-ice formation (Schumacher et al., 1983). Transport

across SL is relatively low compared to most other sections and is higher in summer and highest in November and December. This second peak in early winter may be due, in part, to winter storms that frequently occur in this region (Overland and Pease, 1982) prior to the southward advancement of sea-ice cover, which tends to reduce the impact of wind forcing on the ocean.

Table 1
Bering Sea (region shown in Fig. 1) velocity (cm s^{-1}) statistics computed from monthly mean model output

Time	Minimum	Maximum	Mean	S.D.
23-year mean	3.350E-5	49.661	3.542	3.722
1979 mean	1.637E-4	58.843	4.352	4.449
1994 mean	1.815E-3	38.126	3.258	3.387
1979–1994 mean	2.599E-3	20.738	2.474	2.337
1987–1979 mean	3.503E-3	15.533	1.838	2.027
1987–1994 mean	6.059E-4	17.627	2.133	2.441

Table 2
Statistics based on monthly mean time series of 23-year mean net volume transport through various sections shown in Fig. 1

Section	Mean	Max	Min	S.D.
BS	0.65	1.28	0.11	0.23
AS	0.52	0.95	0.07	0.17
SS	0.13	0.73	-0.20	0.13
AC	0.37	0.97	-0.70	0.22
SL	0.13	1.23	-0.39	0.22

Maximum positive heat transport (referenced to -0.1°C) occurs in summer and early autumn at all sections (Fig. 4B). We chose a reference temperature of -0.1°C because the deeper layers of the northern Bering Sea typically stay below this temperature throughout the year and we are interested in examining the heating above this value. The net amount of heat transported northward across Shpanberg Strait is $\sim 60\%$ of that across Anadyr Strait even though the volume flux through SS is only 25% of AS (Table 3). This is consistent with observations of warmer water in the eastern Bering Sea as compared to the western regions (Coachman, 1987; Grebmeier et al., 1988). In general, the annual cycle of heat transport does not correlate well with volume transport, mainly due to seasonal changes in water temperature.

Freshwater transport (referenced to a salinity of 34.8) is highest in summer for all sections except SL, where it peaks again in late autumn, similar to the annual cycle of volume transport (Fig. 4C). The reference salinity of 34.8 is chosen because this value allows for comparison with other calculations that have been made in other regions of the Arctic and it is estimated as the mean salinity of the Arctic Ocean (Aagaard and Carmack, 1989). Freshwater transport across Bering Strait is lowest in winter and early spring ($30\text{--}40\text{ mSv}$, $1\text{ mSv} = 10^3\text{ m}^3\text{ s}^{-1}$) and

highest in July ($\sim 70\text{ mSv}$) in the annual cycle. The 23-year mean freshwater transport is $\sim 47\text{ mSv}$, with approximately 37 mSv coming from the upstream Anadyr Strait and $\sim 10\text{ mSv}$ coming from Shpanberg Strait. These relative contributions to the BS freshwater transport are similar to the volume transport contributions.

Time series over 23 years for the five vertical sections show seasonal, as well as interannual, variability in flow across the northern Bering shelf (Fig. 5). The net 23-year mean volume transport across Bering Strait is 0.65 Sv , with 0.72 Sv moving northward and a slight but annually regular component (0.07 Sv) moving southward (Table 3 and Fig. 5). An annual minimum of 0.48 Sv was reached in 1994 and a maximum of 0.78 Sv in 1979, thus giving an interannual variability of approximately $\pm 0.15\text{ Sv}$. A similar estimate of $\pm 0.2\text{ Sv}$ was made by Coachman (1993) based on observational studies during the ISHTAR program. Net monthly mean variation in transport is greater than 1 Sv , with a low of 0.11 Sv in December 1997 and a high of 1.28 Sv in August 1999. Examination of instantaneous transports across Bering Strait (calculated every model time-step of 480 s) reveals even stronger wind-driven variability, from 2.7 Sv northward to 2.5 Sv southward (data not shown).

With respect to other sections, SS, AC, and SL all had numerous negative monthly mean minima representative of flow reversals (Fig. 5). The most notable flow reversal (up to -0.70 Sv) in the 23-year time series occurred along the AC section during November and December 2000. Flow continued to be westward across the northwestern Bering Sea until March 2001. This episode was also evident in the AS, SS, and SL sections, with greatly increased northwestward flow across the northern Bering shelf. This event also coincided with observations of reduced sea-ice conditions during winter of 2000–2001 (Fig. 6). Observations mainly derived from satellite data during February 1999 and 2001 show that ice concentrations were very low during 2001 as compared to a more typical year, 1999 (Fig. 6A,B; Clement et al., 2004). The model shows a similar ice distribution in the two years, except for slightly lower ice concentrations ($80\text{--}95\%$) instead of solid $>95\%$ ice cover reported during February 1999 (Fig. 6C,D). These areas of slightly reduced ice cover concentrations in the model might be representative of the realistic presence of leads and relatively warm ocean currents. The strong flow reversal, which peaked in November and December

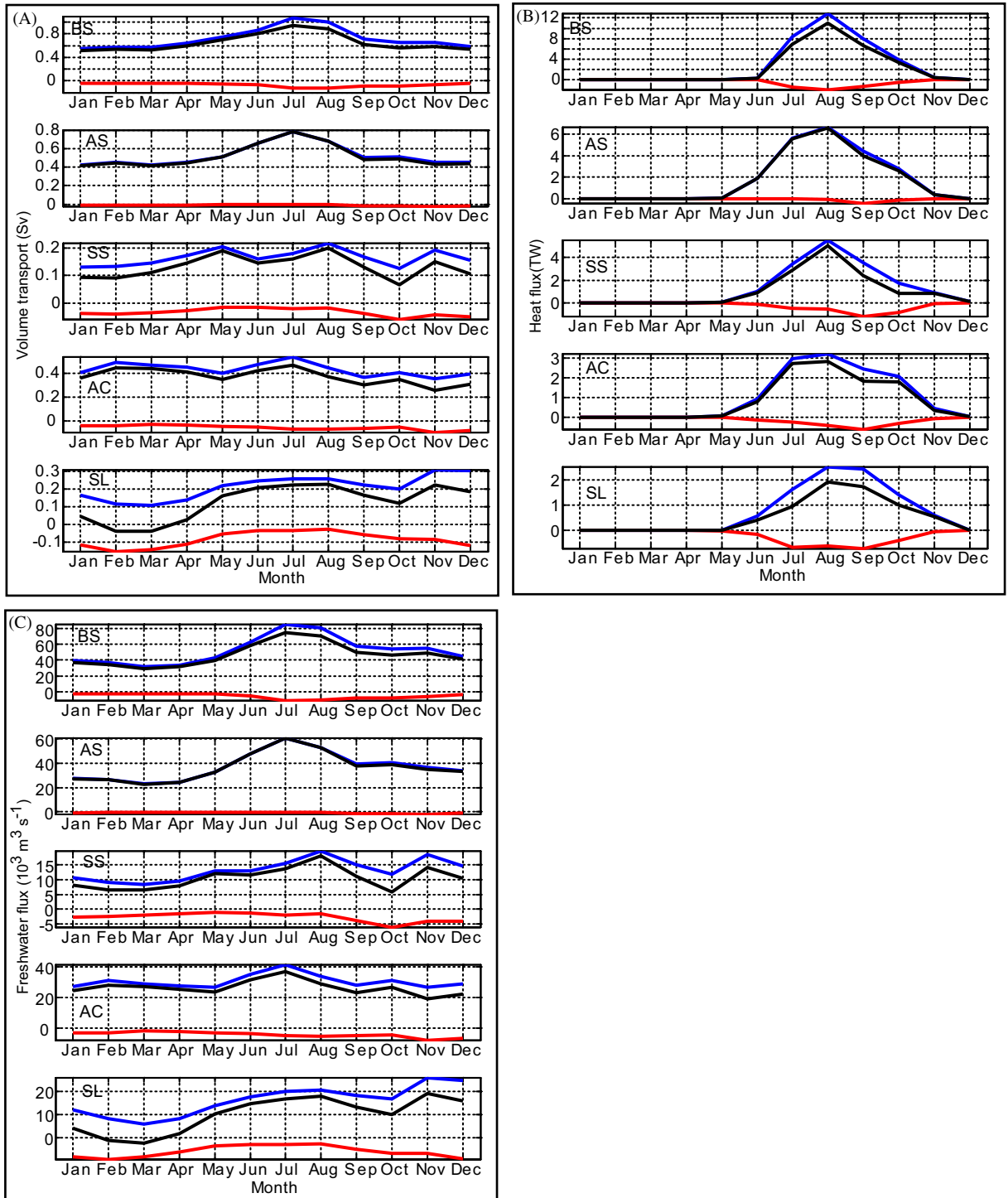


Fig. 4. Modeled annual climatological (A) volume, (B) heat, and (C) freshwater fluxes through northern Bering Sea sections (see Fig. 1 for section locations). Monthly means are calculated from a 23-year time series (1979–2001). Positive (blue line) fluxes represent flow to the North or East according to the model grid (see Fig. 1), while negative (red line) fluxes represent flow to the south or west. Black lines represent net flow. The reference temperature is $-0.1\text{ }^{\circ}\text{C}$ and the reference salinity is 34.8.

Table 3

Twenty-three-year mean volume transport (Vol, Sv), heat transport (Heat, TW), and fresh water transport (FW, $10^3 \text{ m}^3 \text{ s}^{-1}$) through selected sections

Section	Vol Net	Vol In	Vol Out	Heat Net	Heat In	Heat Out	FW Net	FW In	FW Out
BS	0.65 (0.23)	0.72 (0.25)	-0.07 (0.03)	2.37 (4.12)	2.82 (4.78)	-0.45 (0.70)	46.84 (20.44)	52.09 (22.94)	-5.25 (3.21)
AS	0.52 (0.18)	0.53 (0.17)	-0.01 (0.01)	1.75 (2.52)	1.81 (2.55)	-0.06 (0.16)	36.61 (15.65)	37.31 (15.35)	-0.70 (0.92)
SS	0.13 (0.13)	0.17 (0.10)	-0.03 (0.03)	1.09 (2.19)	1.36 (2.24)	-0.27 (0.55)	10.55 (11.82)	13.29 (10.01)	-2.74 (3.24)
AC	0.37 (0.22)	0.43 (0.18)	-0.06 (0.07)	0.86 (1.39)	1.01 (1.48)	-0.15 (0.26)	26.27 (16.52)	30.50 (13.82)	-4.22 (5.76)
SL	0.13 (0.22)	0.21 (0.16)	-0.09 (0.09)	0.55 (1.06)	0.76 (1.11)	-0.22 (0.43)	9.97 (17.27)	15.98 (13.41)	-6.01 (6.15)

Qheat is referenced to -0.1°C and FW is referenced to 34.8 psu. Calculations are for the entire water column. Standard deviation is shown in parenthesis.

2000, and northwestward movement of sea-ice occurred relatively quickly over the course of a few months during winter 2000–2001. The cause of this event is most likely wind forcing, as shown in Fig. 7. While previous studies indicate that prevailing winds are out of the north to slightly northeast in the northern Bering Sea during winter (Muench and Ahlnäs, 1976; Pease, 1980; Overland, 1981), a very different scenario took place during winter 2000–2001. Fig. 7 depicts the ECMWF wind forcing fields used in the model averaged over the 2-month peak in flow reversal (November and December 2000) as compared to the more typical year (November and December 1998; Fig. 5). In 1998, wind was out of the north with speeds of $3\text{--}4 \text{ m s}^{-1}$ in the vicinity of Bering Strait and up to 4.5 m s^{-1} south of St. Lawrence Island. In contrast, during 2000 much stronger wind speeds of $5\text{--}6.5 \text{ m s}^{-1}$ occurred near Bering Strait, with speeds up to 9.3 m s^{-1} in the Gulf of Anadyr. The average magnitude difference between 1998 and 2000 winter winds (Fig. 7C) was 3.0 m s^{-1} and the wind direction was shifted an average of 43° to a more easterly pattern in 2000. Observational measurements from this time period corroborate an unusual wind and resulting ice cover pattern in winter 2000–2001 (Clement et al., 2004). The dramatic response in sea-ice and ocean conditions to this weather pattern suggests that wind is the dominant forcing mechanism in the northern Bering Sea.

We also have examined correlation of the Bering Strait volume transport (13-month running mean of monthly means for 1979–2001) with several time series of large-scale weather indices. The correlation

with the Arctic Oscillation (AO) is negative ($r = -0.51$) with the AO leading Bering Strait transport by three months. Therefore, the AO can explain approximately 26% ($r^2 \times 100$) of the variance in the Bering Strait transport. Bering Strait transport is positively correlated ($r = 0.53$) with the Pacific Decadal Oscillation (PDO) explaining $\sim 28\%$ of the variance, while correlation with the Pacific-North America Index (PNA) is 0.39 explaining $\sim 15\%$ of the transport variance. The time lag that gives the highest correlation with the PDO and PNA is approximately three years. However, the PDO and PNA are not independent as they incorporate similar weather information. Assuming the PDO/PNA and AO are independent, the combined effect of the AO and the PDO/PNA can explain $\sim 54/41\%$ of the total variance of the Bering Strait transport. The complexity of the air–sea interactions between atmospheric forcing and Bering Sea circulation prevents us from pinpointing the mechanisms underlying these correlations. The remaining transport variance ($\sim 46\text{--}59\%$) is likely due to a combination of synoptic and/or local weather patterns, sea-ice conditions, and ocean circulation.

Average heat transport (2.37 TW , S.D. = $\pm 4.12 \text{ TW}$) across Bering Strait indicates a net flux of warm water (relative to the reference temperature of -0.1°C) to the north (Fig. 8A,8B). There were summer peaks upwards of 20 TW when a large flux of warm water transited northward (1979, 1986, 1990, 1994, and 1999). The annual average heat transport ranged from 1.29 (during 1983) to 4.28 TW (during 1979) over a semi-cyclic time period of 3–5 years. Unlike freshwater transport,

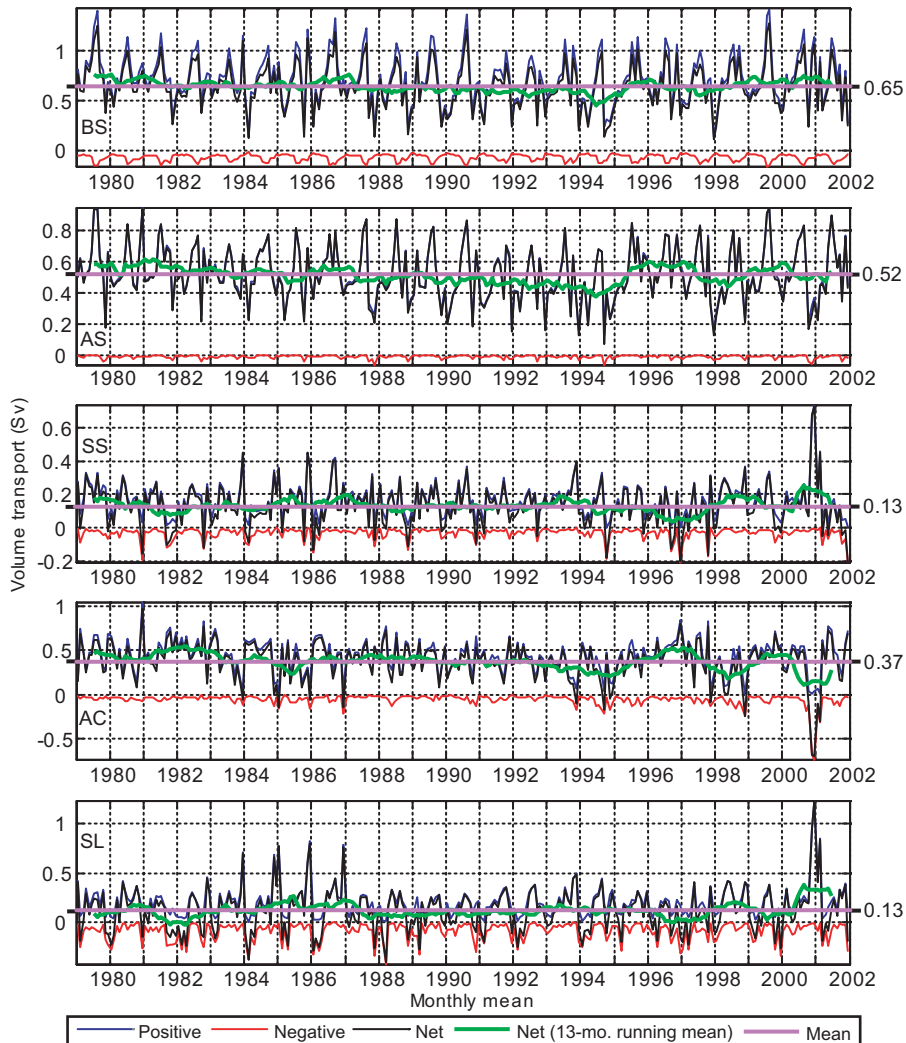


Fig. 5. Monthly mean volume transport over a 23-year time series (1979–2001). Positive fluxes represent flow to the north or east according to the model grid (see Fig. 1), while negative fluxes represent flow to the south or west. The smoothed net flux (thick green line) is a 13-month running mean. The 23-yr mean is shown at the end of each time-series.

heat transport across all the sections does not appear to be directly linked to volume transport, but instead has a unique pattern of variability controlled by changes in both water temperature and flow direction.

The low-salinity, nutrient-rich water flowing northward through Bering Strait is important for maintaining the stratification, as well as constraining nutrient budgets of the Arctic Ocean (Cooper et al., 1997 and references therein). Based on data collected during the 1970s and 1980s (e.g., Coachman and Aagaard, 1988), Aagaard and Carmack (1989) estimate the freshwater inflow to be $\sim 1670 \text{ km}^3 \text{ yr}^{-1}$, referenced against 34.8 psu. Mod-

eled freshwater transport across Bering Strait for 1979–2001 averaged $46,842 \text{ m}^3 \text{ s}^{-1}$ when normalized against salinity of 34.8. This translates into $1477 \text{ km}^3 \text{ yr}^{-1}$ (standard deviation of $\pm 192 \text{ km}^3 \text{ yr}^{-1}$, or $\sim 13\%$) over the 23-year simulation, which is 11.5% less than the freshwater flux estimated from observations based on a total volume flux that is 23% larger than that from the model. Interannual variability in freshwater transport is high with values ranging from 981 (during 1994) to $1955 \text{ km}^3 \text{ yr}^{-1}$ (during 1979). Freshwater transport (Fig. 8B) is highly correlated with volume transport at Bering Strait ($r = 0.93$). High correlations also exist for AS ($r = 0.95$) and SS

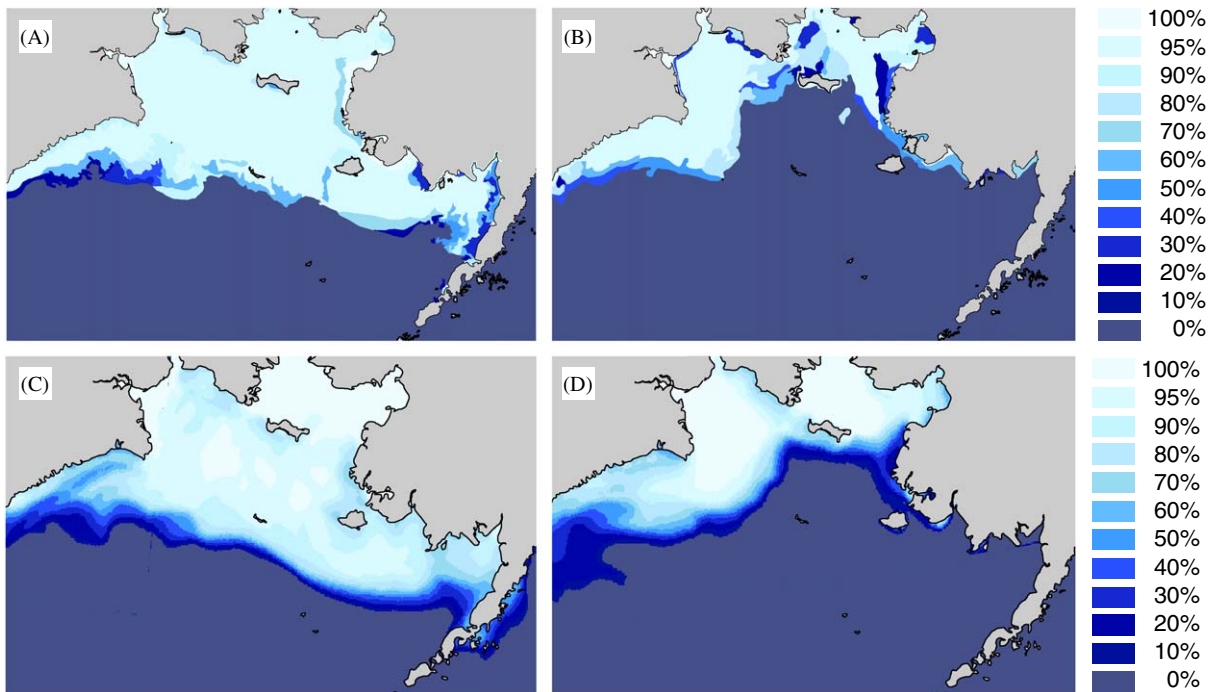


Fig. 6. Sea-ice concentration on (A) February 19,1999 and (B) February 19, 2001 as determined using data obtained from the U.S. National Ice Center (adapted from Clement et al., 2004). Model monthly mean sea-ice concentration during (C) February 1999 and (D) February 2001.

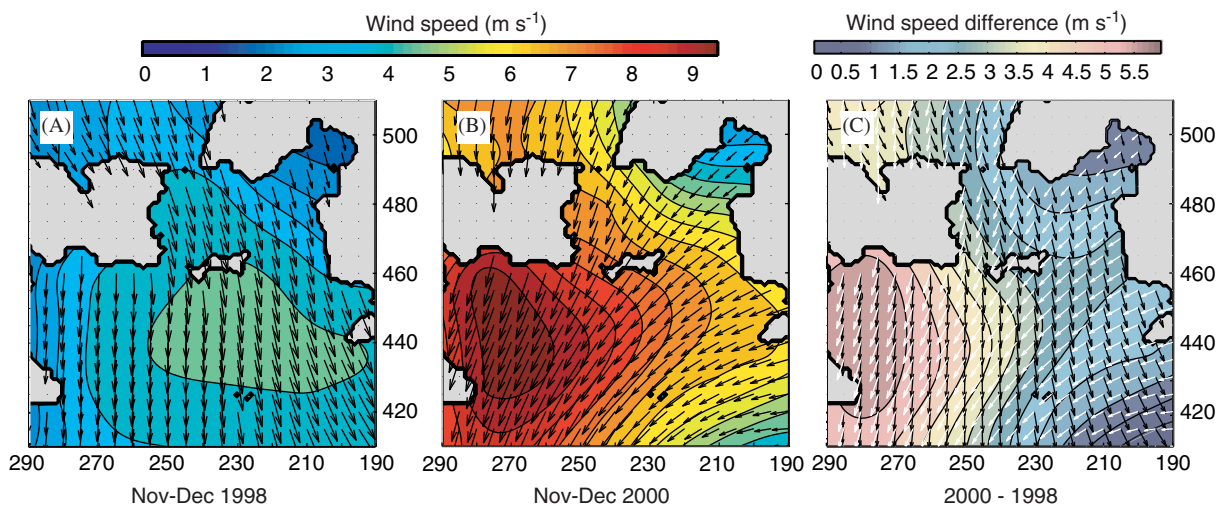


Fig. 7. Model wind forcing fields averaged over November and December (A) 1998 and (B) 2000. (C) The magnitude difference (2000–1998) and both wind fields (1998 in black; 2000 in white).

($r = 0.97$). Anadyr Strait contributes approximately 78% of the freshwater flux through Bering Strait, while Shpanberg Strait contributes the other 22%. These percentage contributions are comparable to the respective percentage contributions of volume transport mentioned earlier.

5. Circulation and water column structure

Flow structure over the northern Bering Sea is complex in both the horizontal and vertical dimensions (Fig. 9A,9B,9C). This is especially true in Bering Strait, where the highest northward

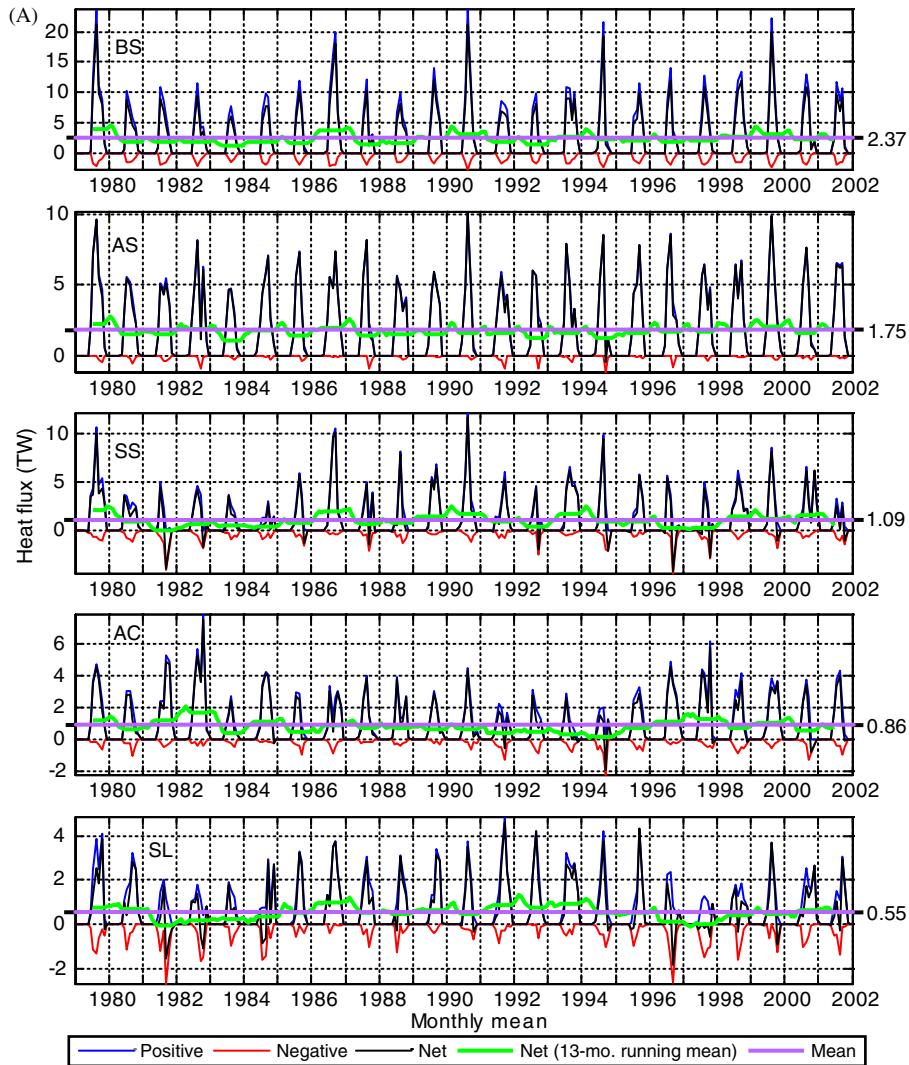


Fig. 8. Monthly mean (A) heat and (B) freshwater fluxes over a 23-year time series. Positive fluxes represent flow to the north or east according to the model grid (see Fig. 1), while negative fluxes represent flow to the south or west. The smoothed net flux (thick green line) is a 13-month running mean. The 23-yr mean is shown at the end of each time-series. The reference temperature is -0.1°C and the reference salinity is 34.8.

velocities (up to 0.45 m s^{-1} in the 23-year mean) occur in the deep channels of the strait, while slower or southward flows occur in the center and closer to the coasts of the 85-km-wide strait. The flow reversal in the center may be due to a stylized representation of the Diomed Islands at this model resolution. A local intensification of the flow is modeled near the western coast, with the 23-year mean velocities greater than 0.10 m s^{-1} , which represents the northward extension of the Anadyr Current upstream. Flow through Bering Strait is most highly correlated with the upstream flow

through Anadyr Strait ($r = 0.83$) and to a lesser degree with Shpanberg Strait ($r = 0.64$). These values are similar to those obtained by Coachman (1993) based on data from current meter moorings in Bering, Anadyr, and Shpanberg Straits. In Anadyr Strait there are two cores of flow with maximum velocities ($>0.06\text{ m s}^{-1}$) at the depths associated with the slopes of the strait and with stronger flow ($>0.10\text{ m s}^{-1}$) along the Siberian side of the slope at depth 10–35 m. Similarly, Shpanberg Strait shows a separation of flow with higher velocity ($>0.05\text{ m s}^{-1}$) near St. Lawrence Island.

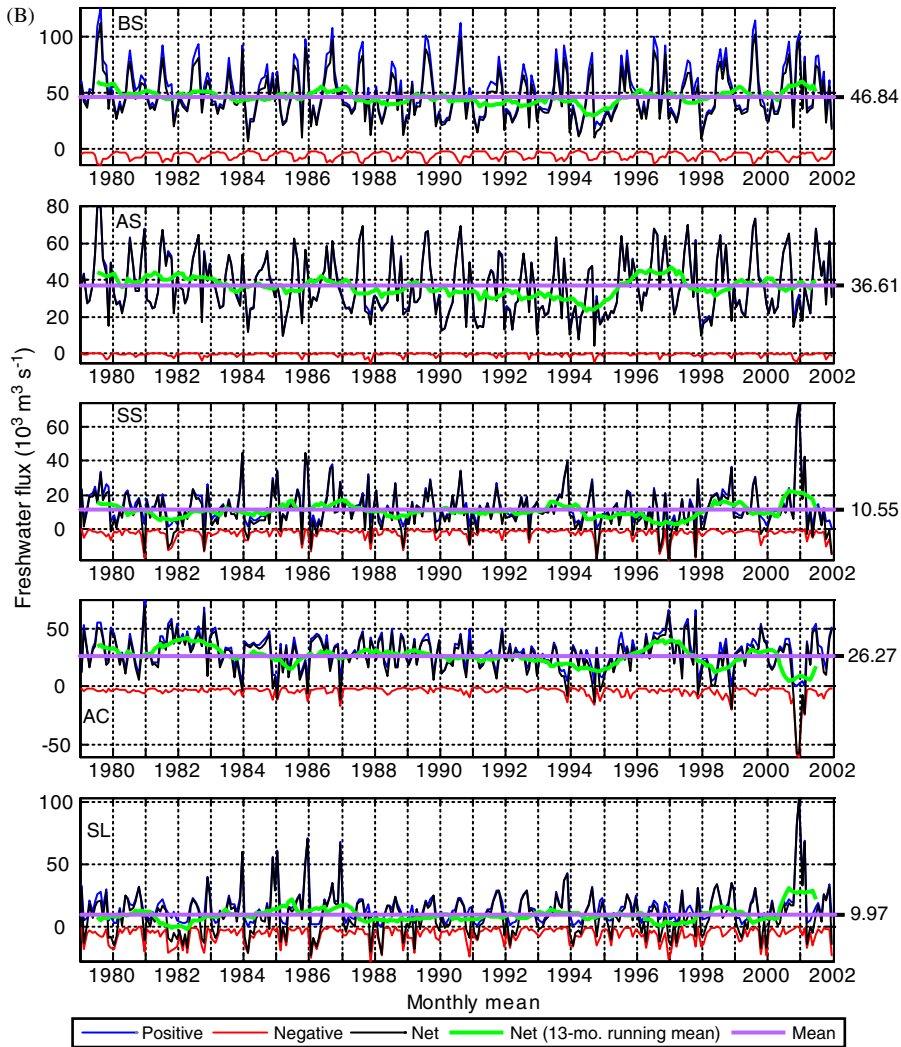


Fig. 8. (Continued)

The Anadyr Current feeding into Anadyr Strait with a velocity core of over 0.12 m s^{-1} in the 23-year mean is represented as a narrow (~ 70 -km-wide) coastal current. The St. Lawrence section shows an eastward flow up to 0.06 m s^{-1} near the island with a sluggish westward flow further offshore.

As discussed earlier, velocity in Bering Strait is seasonally variable, with lower values during winter under sea-ice cover (data not shown). The Bering Strait velocity core is located in the deep western and eastern channels with wintertime monthly mean speeds of 0.2 – 0.4 m s^{-1} . During summer, after the sea-ice is removed, core velocity increases to 0.4 – 0.6 m s^{-1} , and the core vertically extends from near-bottom into shallow water, sometimes up to

the surface (July and August). Throughout the year the eastern channel tends to have higher velocity than the western channel (by ~ 0.05 – 0.15 m s^{-1}). Such differences in velocity and water-mass properties (as discussed below) are especially important when interpreting data only from the U.S. (eastern) side of the strait.

Mean water temperatures for the sections range from -1.8°C near-bottom in the St. Lawrence section to 4°C at the surface in the eastern part of Shpanberg Strait (Fig. 9B). The east–west gradient across Bering Strait is clearly reflected in the colder temperatures from Anadyr Strait to the west and the warmer temperatures from Shpanberg Strait to the east. However, the 23-year mean surface water

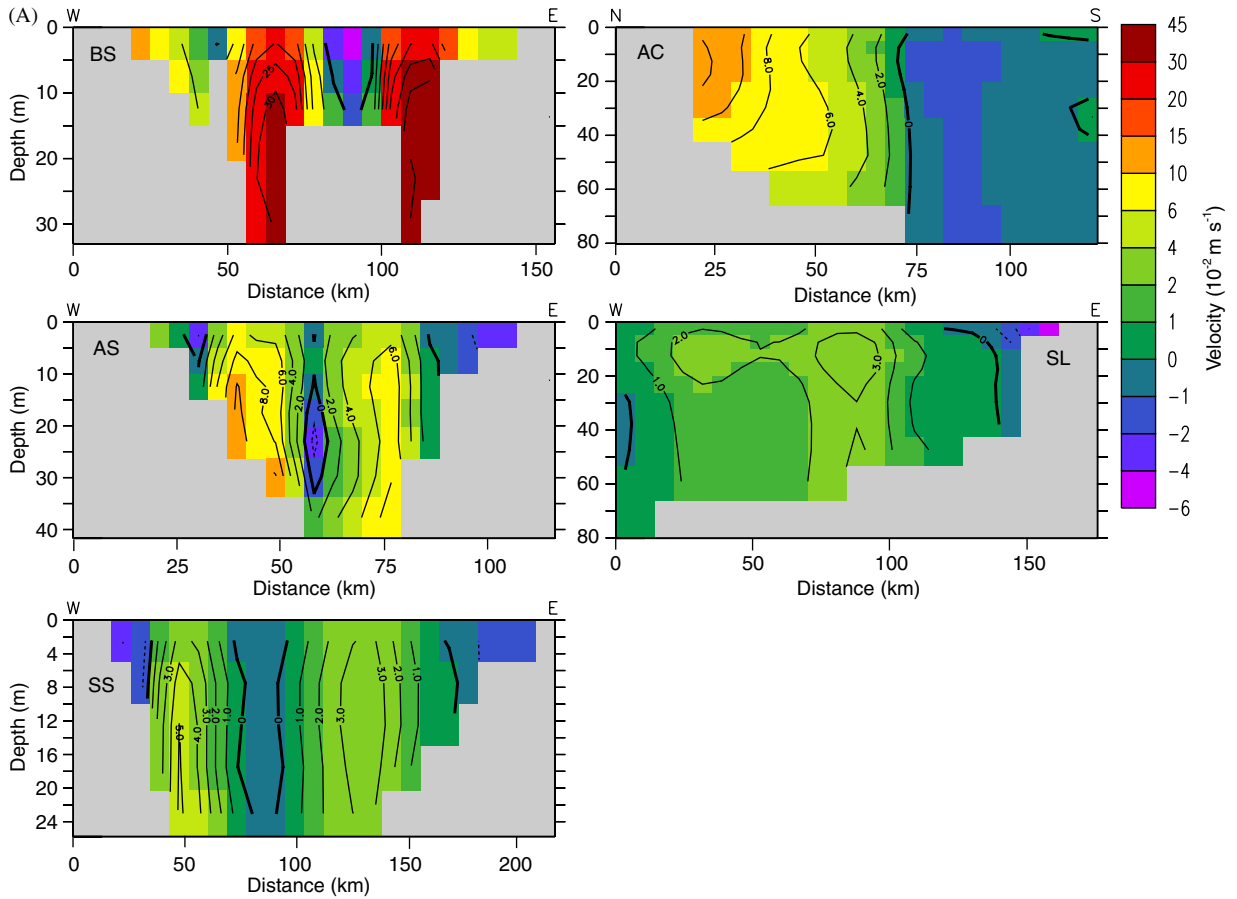


Fig. 9. Twenty-three-year mean profiles for various sections: (A) velocity (m s^{-1}), (B) temperature ($^{\circ}\text{C}$), (C) salinity. Positive velocity is directed northward or eastward (AC).

temperature in both Anadyr and Shpanberg Straits is warmer than Bering Strait surface water temperature. Possible causes of this surface south–north temperature gradient are discussed in Section 9.

Salinity ranges from 31.4 to 33.2 across Bering Strait, with fresher water at the surface and on the eastern side of the section due to the contribution of Alaskan Coastal Water entering through Shpanberg Strait (Fig. 9C). The salinity maximum in the core of Anadyr Current is advected, after a slight dilution, through Anadyr Strait into the deep, western channel of Bering Strait. The high and low salinity signals are moderated as water flows northward toward Bering Strait, which suggests mixing north of St. Lawrence Island. However, an east–west gradient across Bering Strait remains, due to the dominant contributions from upstream water masses.

Twenty-three-year mean seasonal changes in the northern Bering Sea were analyzed at four vertical stations: in the deepest part of Anadyr, Shpanberg,

and Bering (western and eastern channels) straits (Fig. 10; see Fig. 1 for station locations). Temperatures for all stations were isothermal near the freezing point of seawater from December through April (Fig. 10). Surface warming developed first in AS and SS during May and the water temperature reached 10.5°C at the surface by July. The western and eastern channels of Bering Strait followed AS and SS warming, reaching 8 and 10°C , respectively, by August. It is interesting to note that from July to October surface waters in AS and SS were warmer than the downstream Bering Strait, while deeper water remained significantly cooler in the upstream locations. This warming of deeper Bering Strait water (especially in the eastern channel) may be a result of warm water coming from Norton Sound and subsequent mixing between St. Lawrence Island and Bering Strait. The bottom of the thermocline was at $\sim 10 \text{ m}$ in July and deepened to 15–20 m in September.

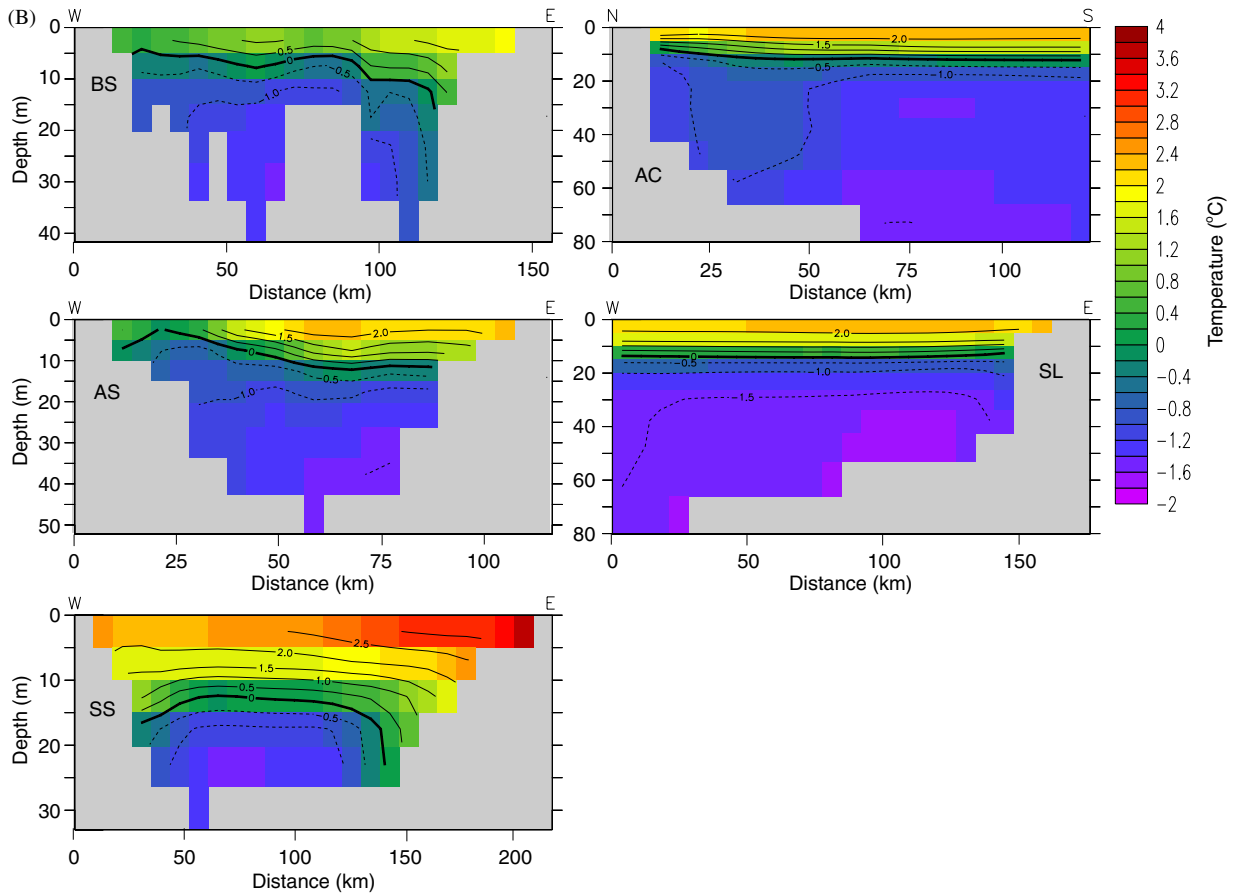


Fig. 9. (Continued)

During winter, the stations show very little vertical salinity structure (figure not shown); however, as ice melt begins during spring, SS begins to develop a low-salinity surface layer in April with other sections following in May and June. The eastern channel of Bering Strait has the lowest surface salinity ($S = 30$) in July, as peak river discharges from the Yukon and other Alaskan rivers are entrained within the northward flowing Alaska Coastal Current. The density profiles (figure not shown) are very similar to the salinity profiles, which is not surprising at low temperatures. The monthly mean density (over 23-years) across the Bering Strait section shows a persistent east–west gradient over the entire year with higher density to the west (not shown). Stronger stratification sets in during June, primarily due to sea-ice melt and runoff, and lasts through September and October.

As mentioned earlier, vertical sections of temperature (Fig. 9B) indicate the possibility of vertical

mixing, leading to warming of deeper water after it passes through AS and SS. Alternatively, or perhaps in addition, the cooling in the upper water column north of St. Lawrence Island in the Chirikov Basin could be involved. To examine the possibility of these processes, we provide a T–S plot for the three main sections (AS, SS, and BS; Fig. 11). This shows that waters at BS are similar to AS with slightly lower density near the surface because of the SS influence. For depth levels 12.5 and 17.5 m, BS is actually denser than AS, suggesting the possibility of cooling and/or sea-ice formation north of St. Lawrence Island.

6. Model-data validation at Bering Strait

Three moorings in the vicinity of Bering Strait have produced time series of velocity, salinity, and temperature (Roach et al., 1995; Woodgate et al., 2005). Mooring locations were in the western

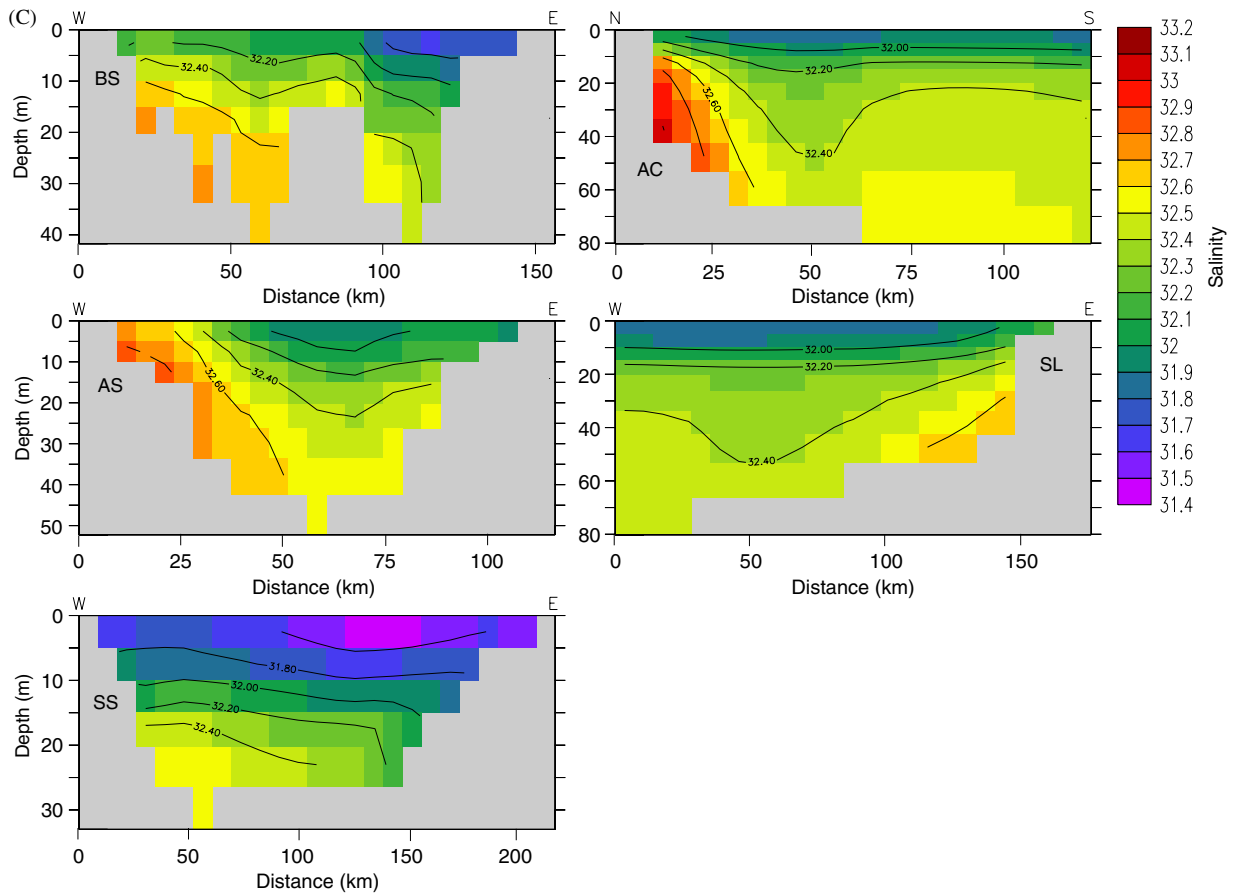


Fig. 9. (Continued)

channel, eastern channel, and just north of Bering Strait with instruments placed approximately 10 m above the bottom (locations shown in Fig. 1). There has been only limited access to the western channel location through international collaboration, because it lies in Russian territorial waters. First, we compare salinity and temperature data for 1990–2001 (courtesy of Woodgate et al., 2005) with model output for 1979–2001 (Fig. 12). There is a clear seasonal cycle in salinity and temperature from both the observational and model time series. Results show that the modeled salinities are within the range of the observations, but there is somewhat less variability in the model output. The observational data show a salinity range of approximately 1.5 psu over each annual cycle, while the model range is only about 1.2 psu. Modeled salinities also tend to be higher than observations. A significant peak in salinity during 1991 is reflected in both the modeled and observational time series. Over the annual cycle, temperatures have a range of approxi-

mately 2–6.5 °C in the model output, while in the observational dataset the range is 4–8 °C. In both the model output and the observational data the eastern channel is almost always warmer than the western channel and northern location. Summer temperatures in the western channel and to the north are generally lower in the model than in observations. In the eastern channel, the modeled temperature agrees quite well with the data; however, there are some years when the model shows colder temperatures in summer. It is possible that the depth at which the observations were made and the model depth may be inconsistent and could lead to different values of salinity and temperature shown in Fig. 12. In addition, observations are made at a single depth compared to modeled values representing a layer with thickness ranging from 5 to 10 m in the upper 50 m.

An important time scale to consider in the Bering Strait volume transport is the annual cycle. We show the available estimates adapted from

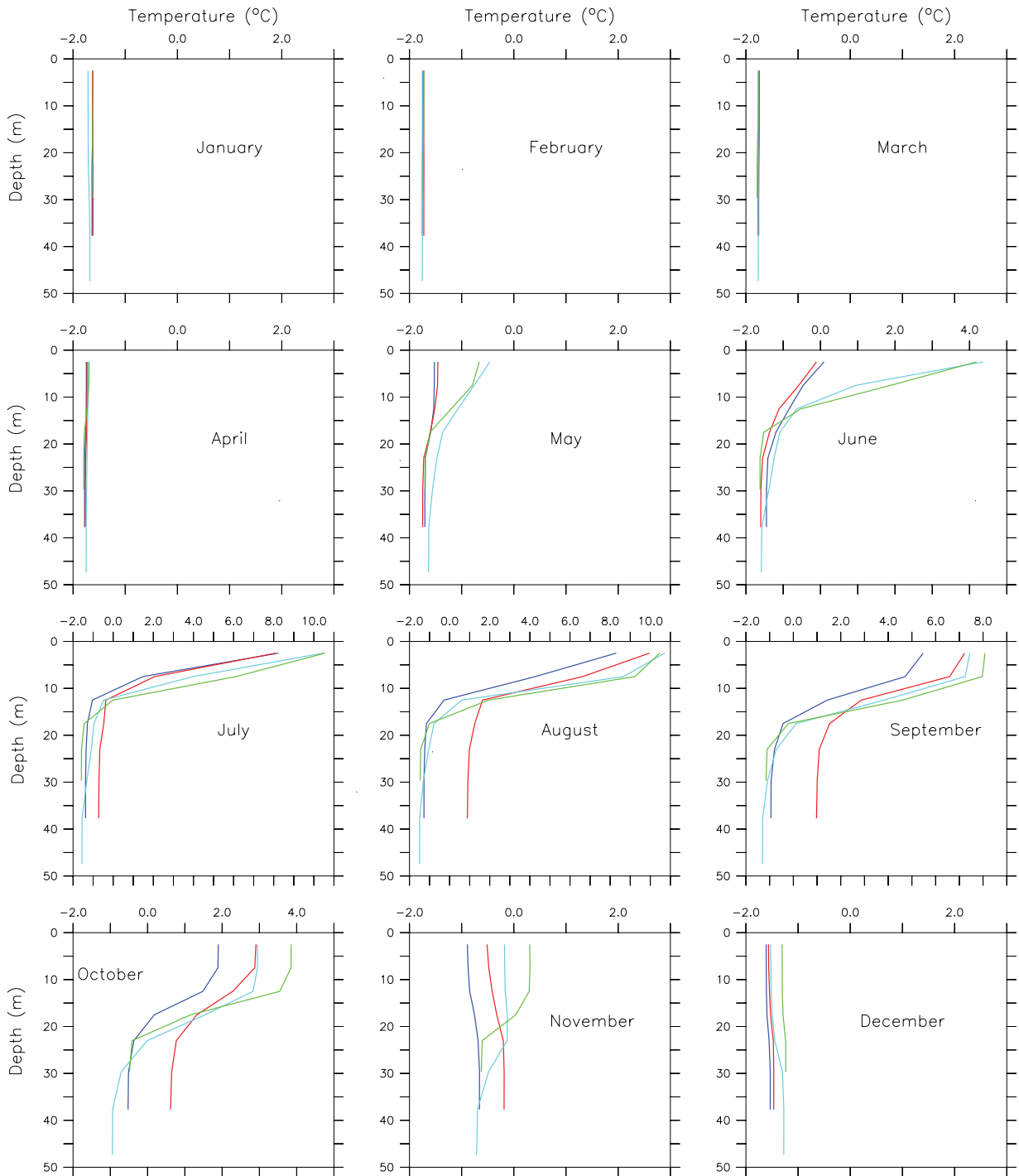


Fig. 10. Monthly mean vertical profiles of temperature (°C) at various model stations taken at the deepest point in each channel or strait (see Fig. 1). The stations are the east (red) and west (dark blue) channels of Bering Strait, Anadyr Strait (light blue), and Shpanberg Strait (green).

Coachman and Aagaard [1988; herein after referred to as C&A (1988)] and Roach et al. (1995), along with model estimates calculated via two different

methods (Fig. 13). The first method is an integral of velocity multiplied by sectional area at each model grid point along the Bering Strait section. The

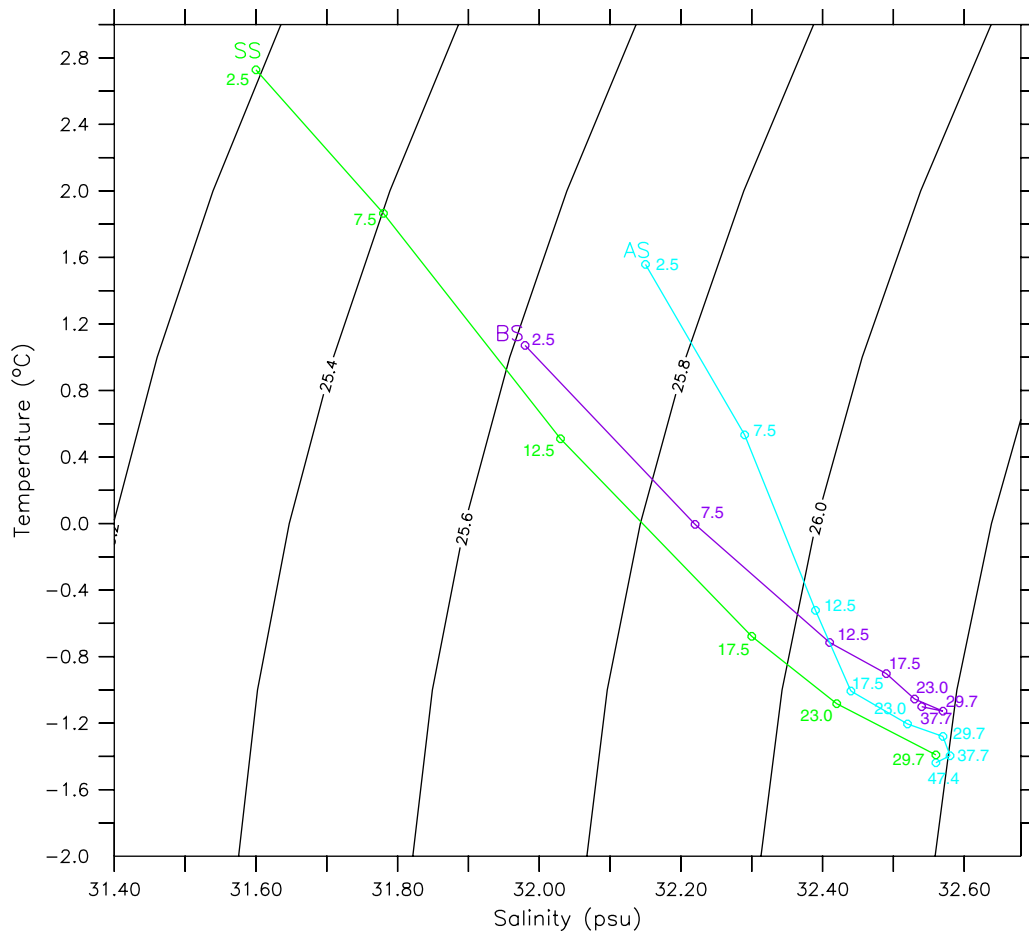


Fig. 11. Twenty-three-year mean T–S diagram. Numbers represent the depth of each section. T–S values are a horizontal mean across each section. Bering Strait (purple), Anadyr Strait (blue), and Shpanberg Strait (green).

second method represents the product of velocity at a single point near the bottom of the Eastern Channel (i.e. the location of eastern mooring from Roach et al., 1995, and Woodgate et al., 2005) and a constant cross-sectional area (2.6 km^2). This second calculation allows direct comparison with observational estimates based on the same method (Woodgate et al., 2005) using velocity from the single deep mooring in the eastern channel. The methods of Roach et al. (1995) are less straightforward; however, results suggest they are similar to those of Woodgate et al. (2005) except they combine intermittent velocities from three near-bottom moorings in and north of Bering Strait during October 1990–October 1994 and use regression techniques to fill in assorted gaps in the data. The C&A (1988) estimate is based on various short-term (less than one year) measurements and correlation with the wind field from 1946 to 1985. The Roach

et al. (1995) study also extends C&A (1988) estimations from geostrophic wind through 1992. All four estimates are similar in that they show higher transport in summer and lower values in winter (Fig. 13). The modeled transports are most similar to the C&A (1988) estimates and are typically within one standard deviation of these observations. Exceptions are during May, when the second method is slightly higher and during June and July, when the first method is slightly lower. The Roach et al. (1995) estimate has a more pronounced annual cycle and is in excess of one standard deviation above the C&A (1988) estimate during May–July.

Expanding the comparison of the two methods for calculating the modeled transport, we observe that an estimate derived as a product of velocity at a single point and a constant cross-sectional area (method 2; as in Woodgate et al., 2005) yields an

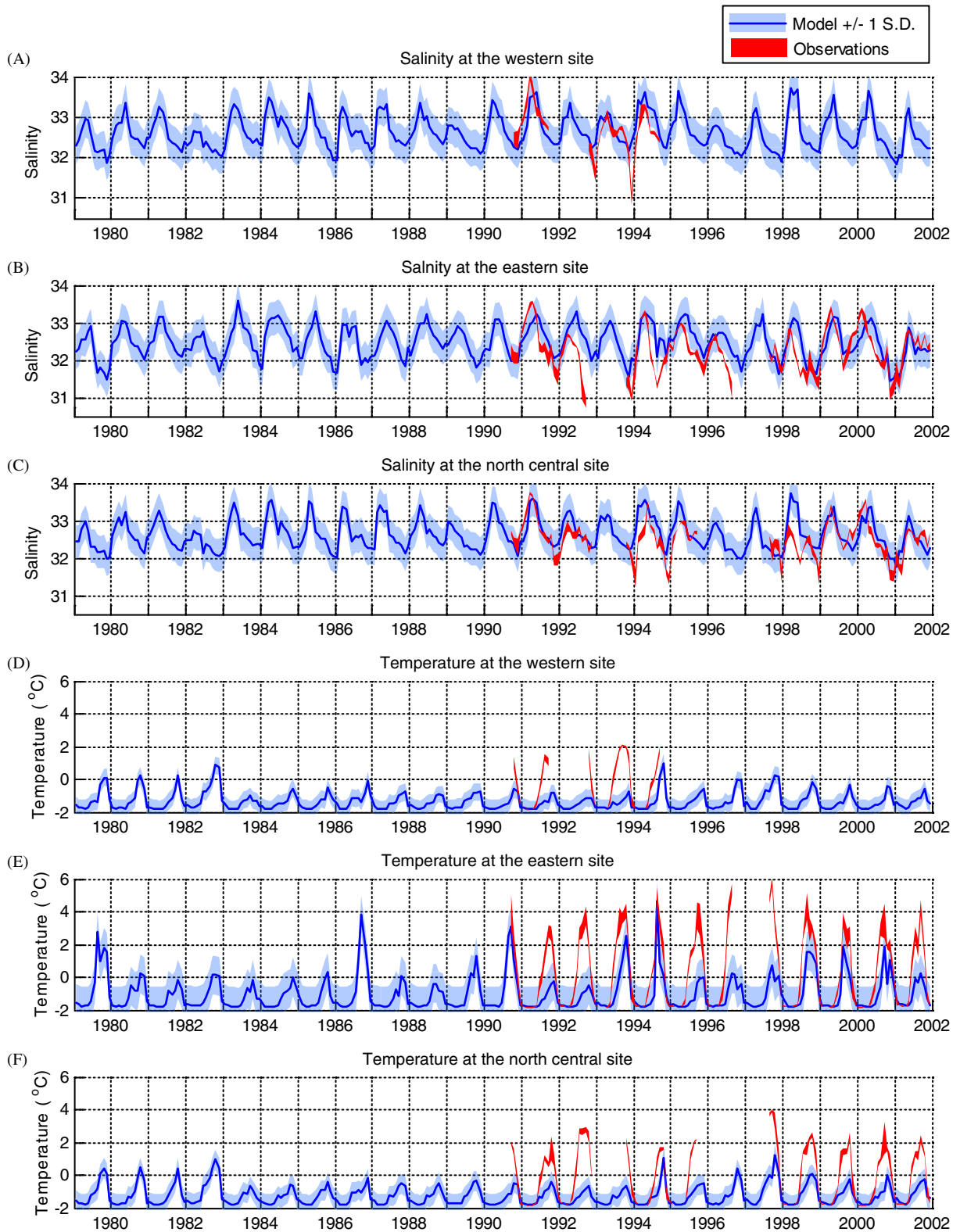


Fig. 12. Bering Strait monthly mean salinity and temperature from the model (blue) and as measured at three moorings at approximately 10 m above the bottom (red). Salinity at the (A) western site, (B) eastern site, and (C) north central site. Temperature at the (D) western site, (E) eastern site, and (F) north central site. Light blue shading indicates ± 1 S. D. for the model estimates. Mooring observations include physical errors. Mooring data is courtesy of Woodgate et al. (2005).

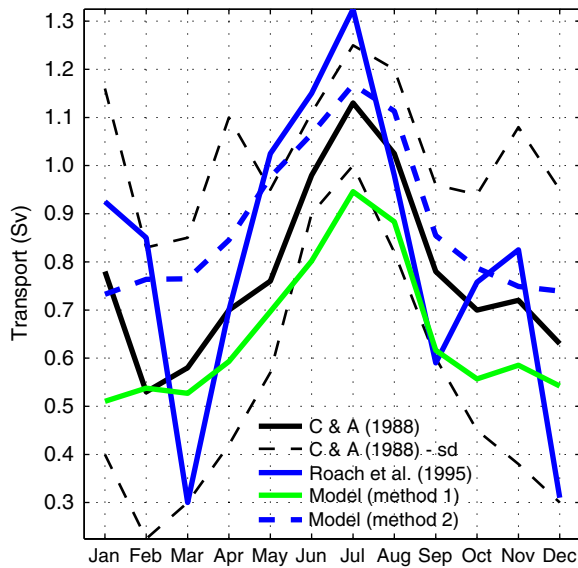


Fig. 13. Bering Strait annual cycle transport (monthly means) from various studies. The Coachman and Aagaard (1988) estimate is shown in black with standard deviation lines in dashed black. The Roach et al. (1995) estimate is shown as a solid blue dash-dot line. The model estimates were made via two methods. The first method (green) utilizes the entire strait in both the horizontal and vertical directions and is the method used for other calculations in this paper. The second method (dashed blue) is done by using only the near-bottom velocity in the eastern channel multiplied by a cross-sectional area (2.6 km^2).

average transport of 0.802 Sv for the period October 1990–October 1994 (Fig. 14). This value is close to the observational estimate of 0.83 Sv reported by Roach et al. (1995; Fig. 11). The other model method (method 1), which utilizes velocity information for the entire strait, yields a lower transport of 0.582 Sv or $\sim 73\%$ of the first method estimate. Therefore, we conclude that estimates utilizing only one point measurement of near-bottom velocity in the eastern channel of Bering Strait may overestimate the volume transport through the strait by up to 27%.

Bering Strait transport varies also at the inter-annual time scale. As in Fig. 13, we present three observational estimates of annual mean values adapted from previous studies along with the model results in Fig. 15. In addition, we also show some recent estimates based on velocities in the Eastern Channel and north central moorings (and the constant cross-sectional area, as previously mentioned). These estimates are courtesy of Woodgate and are based on data presented in a recent paper (Woodgate et al., 2005). The modeled transport

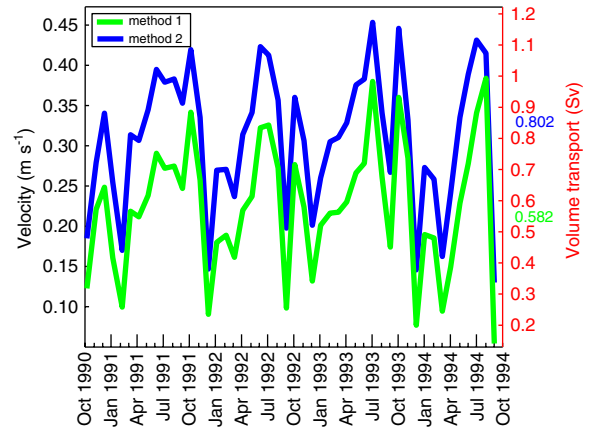


Fig. 14. Bering Strait monthly mean transport during October 1990–October 1994 estimated from the model using two methods. The first method utilizes the entire strait in both the horizontal and vertical directions and is the method used for other calculations in this paper. The second method is done by using only the near-bottom velocity in the eastern channel multiplied by a cross-sectional area (2.6 km^2). Means for the time series are shown on the right axis in the respective colors.

(green line, method 1) on average represents 88% of the observational estimates during 1979–1994, ranging from 34% in 1994 to 115% in 1980. (For this calculation, observational estimates were averaged when more than one estimate occurred.) The simpler model method (dashed blue line, method 2) on average represents 117% of the observational estimates during 1979–1994, ranging from 60% in 1994 to 157% in 1980. The model estimates for 1990–1994 using this method are in a similar range as the observational estimates (0.68 – 1.14 Sv); however, particular annual means do not necessarily overlap. It is important to note here that the Roach et al. (1995) estimate for 1994 did not include October–December, which typically have lower monthly mean transport values. This may partially account for the relatively high transport value reported for 1994. Similarly, the 1990 mean estimate is based on October–December data only, which explains its lower value. Additional uncertainty with comparison of model and Roach et al. (1995) estimates has to do with regression methods used to determine vertical velocity shear and transport during gaps in direct measurements in the deep channels of the strait. When examining the annual mean transport values, it appears that the model (method 1) is most similar to observations from 1979 to 1988 and, in fact, during that time the model estimates average 98% of observational estimates

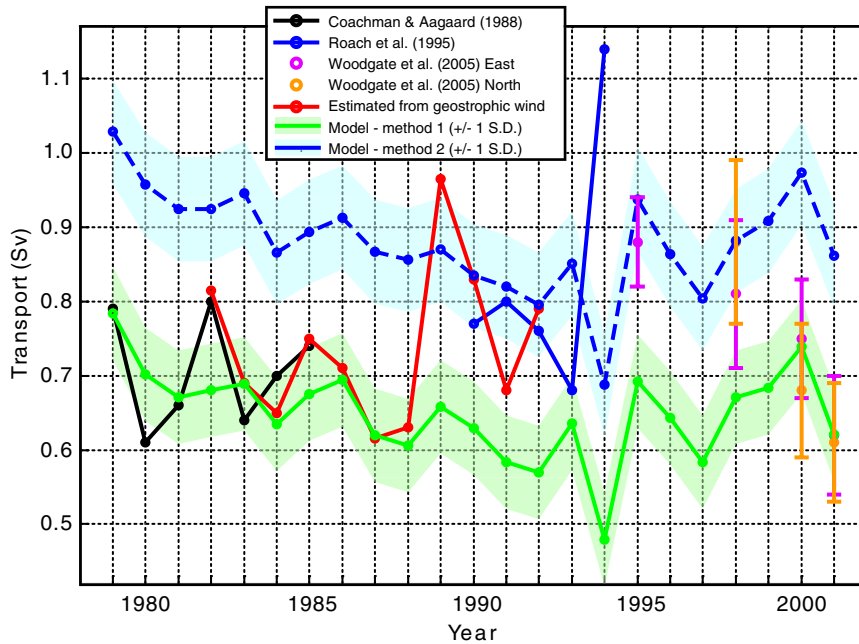


Fig. 15. Bering Strait annual mean transport from various studies during 1946–2001. The Coachman and Aagaard (1988) estimate is a solid black line and the Roach et al. (1995) estimate is a blue line. The estimation from geostrophic wind (red line) was given in Roach et al. (1995). Estimates from Woodgate et al. (2005) are shown as purple (eastern channel mooring) and orange (north central mooring) circles. These estimates include error bars. The model estimates were made via two methods. The first method (green line) utilizes the entire strait in both the horizontal and vertical directions and is the method used for other calculations in this paper. The second method (dashed blue) is done by using only the near-bottom velocity in the eastern channel multiplied by a cross-sectional area (2.6 km^2). For the model estimates, the shading represents $\pm 1 \text{ S. D.}$

(ranging from 84% in 1982 to 115% in 1980). The recent estimates made by Woodgate et al. (2005) tend to fall between the two methods of calculation from the model output. Annual mean volume transport based on data from the Eastern Channel (magenta circles) can be higher or lower than transport based on data from the north central mooring (orange circles). Associated errors in all observational and model datasets make distinguishing between years difficult.

7. Eddy kinetic energy in 1987

With a horizontal grid cell spacing of approximately 9 km, this model is able to resolve eddies with diameters as small as 36 km. As such, we have examined the eddy kinetic energy ($\text{EKE} = (u'^2 + v'^2)/2$) distribution in the Bering Sea calculated from daily fluctuations (u', v'), referred to the 23-year mean. EKE is an important model parameter, which, in the physical world, commonly represents regions of active mixing and associated increased biological productivity. Realistic representation of

EKE in a model is often challenging but when achieved can provide useful information about the dynamics and productivity in a region. Observational estimates of EKE on the Bering shelf are not readily available, hence the following discussion serves to establish a quantitative, yet possibly incomplete, reference.

The mean velocity components for 1979–2001, \bar{u} and \bar{v} , were calculated and then subtracted from the 1987 daily velocity values to obtain u' and v' . We chose the year 1987 because it was characterized by an average transport through Bering Strait and it does not appear strongly biased toward any particular climate regime in the North Pacific or Arctic Ocean. At the surface (0–5 m), annual mean EKE is highest (up to $2700 \text{ cm}^2 \text{ s}^{-2}$) in Bering and Anadyr straits and along the slope in the vicinity of the BSC (Fig. 16A). Lesser, but still significant EKE of approximately $60 \text{ cm}^2 \text{ s}^{-2}$, is found across the middle shelf. Below the wind-driven, surface layer at 20–26 m, we observe much reduced EKE across the middle shelf with some weak intensification along isobaths (Fig. 16B). However, EKE remains very

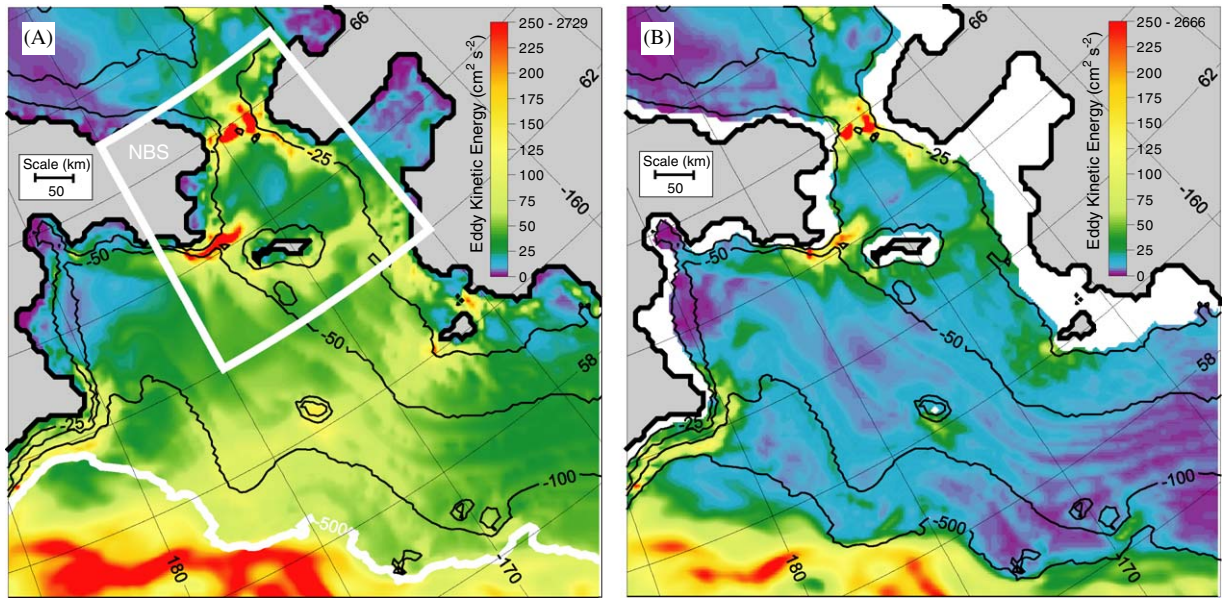


Fig. 16. Annually averaged eddy kinetic energy ($\text{cm}^2 \text{s}^{-2}$) calculated from daily 1987 snapshots (against 23-year mean): (A) surface level, (B) 20–26 m (level 5).

high (up to $2600 \text{ cm}^2 \text{ s}^{-2}$) along the slope and in the northern Bering Sea, especially in Bering and Anadyr straits.

Seasonal changes in EKE in the surface layer are visible across the Bering shelf, with highest values in autumn and winter (Fig. 17). Bering and Anadyr straits maintain relatively high EKE throughout the year, but peak during autumn. The area directly south of St. Lawrence Island is also a region of increased EKE, while north of the island in the Chirikov Basin we observe a distinct decrease. Below the surface at 20–26 m depth, there is a sharp decrease in EKE across the middle shelf (Fig. 18), similar to the annual mean. Again, the EKE in the northern straits and along the BSC remains elevated.

Upon noting the differences in EKE for various regions of the Bering Sea, we computed a daily area-averaged EKE for the northern Bering Sea, the middle shelf, and the entire region (Fig. 19). The northern Bering Sea (NBS) region, defined in Fig. 16A, shows relatively low surface EKE in the first part of 1987, while the middle shelf region has high EKE, likely due to passing storms and ice-edge location (Fig. 19A). Spring EKE is low for all regions followed by a strong increase in the NBS during summer. Finally, the autumn season shows the highest values for the NBS with peaks lasting approximately 5–10 days, a synoptic period similar

to the duration of Bering Sea cyclonic systems. Similar peaks show up for the middle shelf and the entire region, but they are only about two-thirds the magnitude of that observed in the NBS. Below the surface at 20–26 m, the highest EKE for most of the year, except for the NBS in autumn, is over the entire region (Fig. 19B). This is likely due to the strong influence of eddies of the BSC propagating along the slope and into the basin. The middle shelf is much lower in energy throughout most of the year. Using a regional model of the southeastern Bering Sea, Hermann et al. (2002) also found frequent eddy activity along the BSC and much less on the shelf. The shallow shelf waters of the NBS continue to have the highest energy during autumn with deeper water (20–26 m) peaks that are approximately half those at the surface.

8. Comparison with observations of salinity and nutrients

Comparisons of the modeled salinity field were made against field observations from eight cruises during the period 1988–1999 from April through September (Fig. 20A,20B). In this analysis we compare the salinity at the deepest field sample depth or at the lowest model level (which most likely are not the same). In the observational dataset, the deepest sample depth is approximately 5–10 m

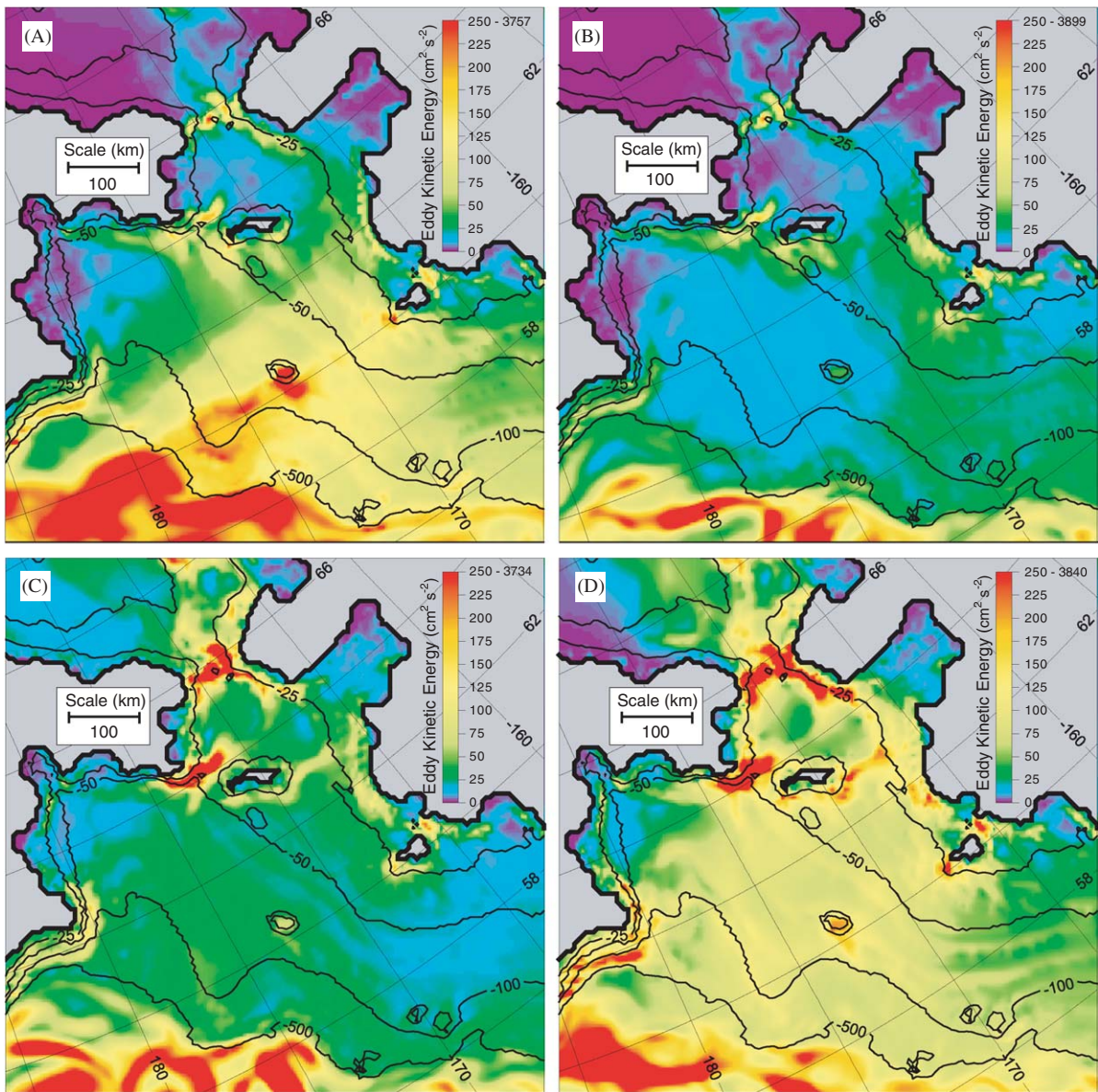


Fig. 17. Seasonally averaged EKE at the surface calculated from daily 1987 snapshots (against 23-year mean): (A) Winter (J–F–M) average, (B) Spring (A–M–J) average, (C) Summer (J–A–S) average, (D) Autumn (O–N–D) average.

above the seabed and the deepest level in the model represents a layer from 5 to 70 m thick in the upper 400 m where almost all observations occur. Note, that salinity is correlated with nutrient concentrations in the Bering Sea in the deeper parts of the water column and/or below the euphotic zone (present study statistics and discussion to follow; Phyllis Stabeno, pers. comm.). Therefore, a significant correlation between the modeled and observed salinities may give insight into the deeper water column nutrient concentrations in the Bering Sea.

A significant (significance level, $\alpha = 0.01$) correlation occurs between observed and modeled salinity in all of the eight cruises combined (sample size = 346; correlation coefficient, $r = 0.47$, p -value < 0.01). The p -value is a measure of how much evidence we have against the null hypothesis (i.e. a small p -value means the correlation is significant). Correlation coefficients for individual cruises range from -0.32 in June 1990 to 0.96 during September 1990. The mean salinity difference for all cruises combined is 0.246 , with the model having higher salinity than

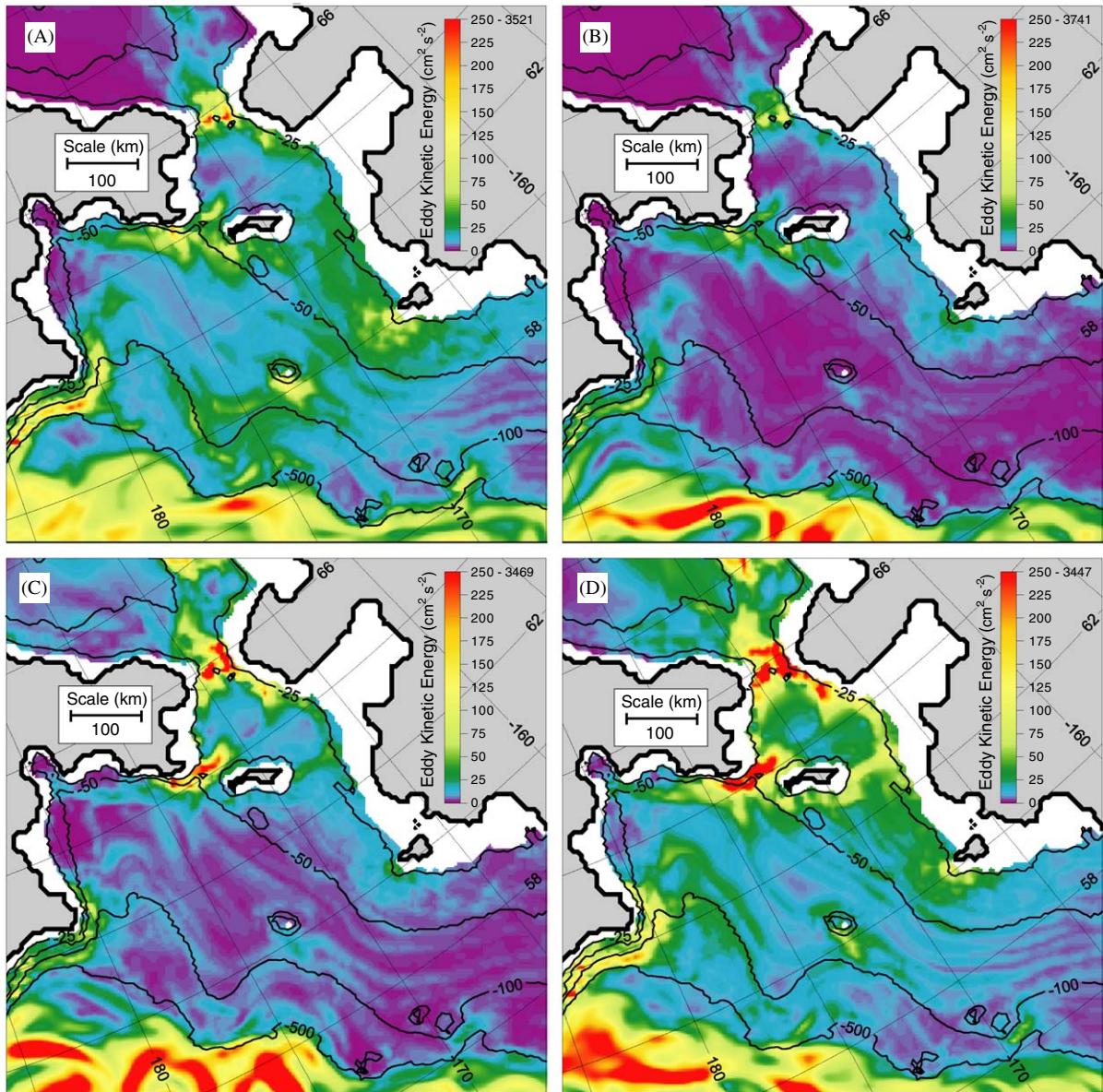


Fig. 18. Seasonally averaged EKE at 20–26 m (level 5) calculated from daily 1987 snapshots (against 23 yr mean): (A) Winter (J–F–M) average, (B) Spring (A–M–J) average, (C) Summer (J–A–S) average, (D) Autumn (O–N–D) average.

observations. For individual cruises, the salinity difference ranges from -0.226 in August 1993, when the model is less saline than observations, to 0.949 in September 1990, when the model is more saline than observations. We note here that a strong correlation is not always associated with a small mean-salinity difference and vice versa.

In general, the model agrees with observations showing fresher water in the east and more saline water in the west (Fig. 20), although there appears

to be a deficit of the freshwater flux in the Alaska Coastal Current in the model. This and other relatively narrow coastal currents may not be fully resolved at the present resolution (e.g. Maslowski and Walczowski, 2002). With respect to the freshwater input, the model directly incorporates runoff from the Yukon River, but not from the Kuskokwim, Naknek and other more southerly sources. In the model, relatively fresh water is found near the coast, but is likely constrained to a narrower path

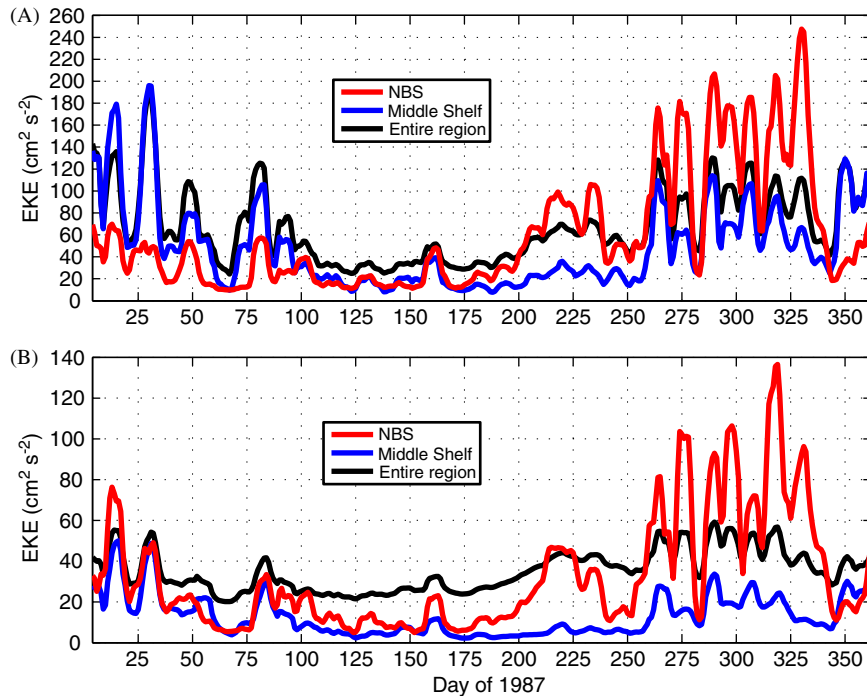


Fig. 19. Daily variability of Bering Sea (area-averaged) EKE during 1987 (against 23-yr mean): (A) surface level, (B) 20–26 m (level 5). Data are presented with 7-day smoothing. Entire region (black line), Northern Bering Sea (NBS; red line), mid-Bering shelf (south of the NBS region with depth less than 500 m; blue line). See Fig. 16a for region boundaries.

than in reality. For example, a horizontal freshwater intrusion extends along the bottom from about 30–70 m depth from the southeast toward the northwest (Fig. 20). The extent and intensity of this tongue of freshwater exhibits seasonal and inter-annual variability. Modeled salinities are generally in a smaller range than the observations; therefore, east–west gradients are somewhat muted in the current version of the model. However, it is important to note that field observations for each cruise were collected instantaneously at individual stations over the course of approximately one month, while the model output is the mean salinity of one month. In addition, the field observations are sampled from water that is approximately 5–10 m above the bottom, which may or may not be the same depth as the deepest model grid level. Also the bottom boundary layer physics occur in the model in a vertical layer, which is thicker than the real boundary layer in most cases.

Finally, we analyze a relationship between observed nutrients (i.e. silicate) and salinity to show potential utility of using model salinity and EKE information as a proxy for nutrient distribution in deep shelf waters. The shelf of the northern Bering

Sea is supplied by upwelling of high-silica water from the deep basin (Tsunogai et al., 1979). Near-bottom field observations of silicate concentrations (Fig. 21) and salinity (Fig. 20) over the Bering shelf have a similar distribution. In fact, a significant correlation exists between the two parameters (sample size = 340; $r = 0.56$; $p < 0.01$) when data from all cruises are combined. The correlation coefficients for individual cruises are between 0.60 and 0.78, except in September 1990 when the correlation coefficient was 0.43. This is possibly due to the extremely low salinity that was present in the east just north of the Seward Peninsula, likely due to a strong mixing of the river runoff signal.

In general, the analyzed silicate concentration has an apparent east–west increase across the Bering shelf. As already mentioned, western and/or deeper stations have higher silicate concentrations due to the upwelling of nutrient-rich deep Bering Sea Water. High silicate concentrations are measured in the Gulf of Anadyr and become diluted and biologically utilized downstream, as this water moves northward toward Bering Strait. The significant correlation between observed salinity and silicate concentration supports the idea that salinity

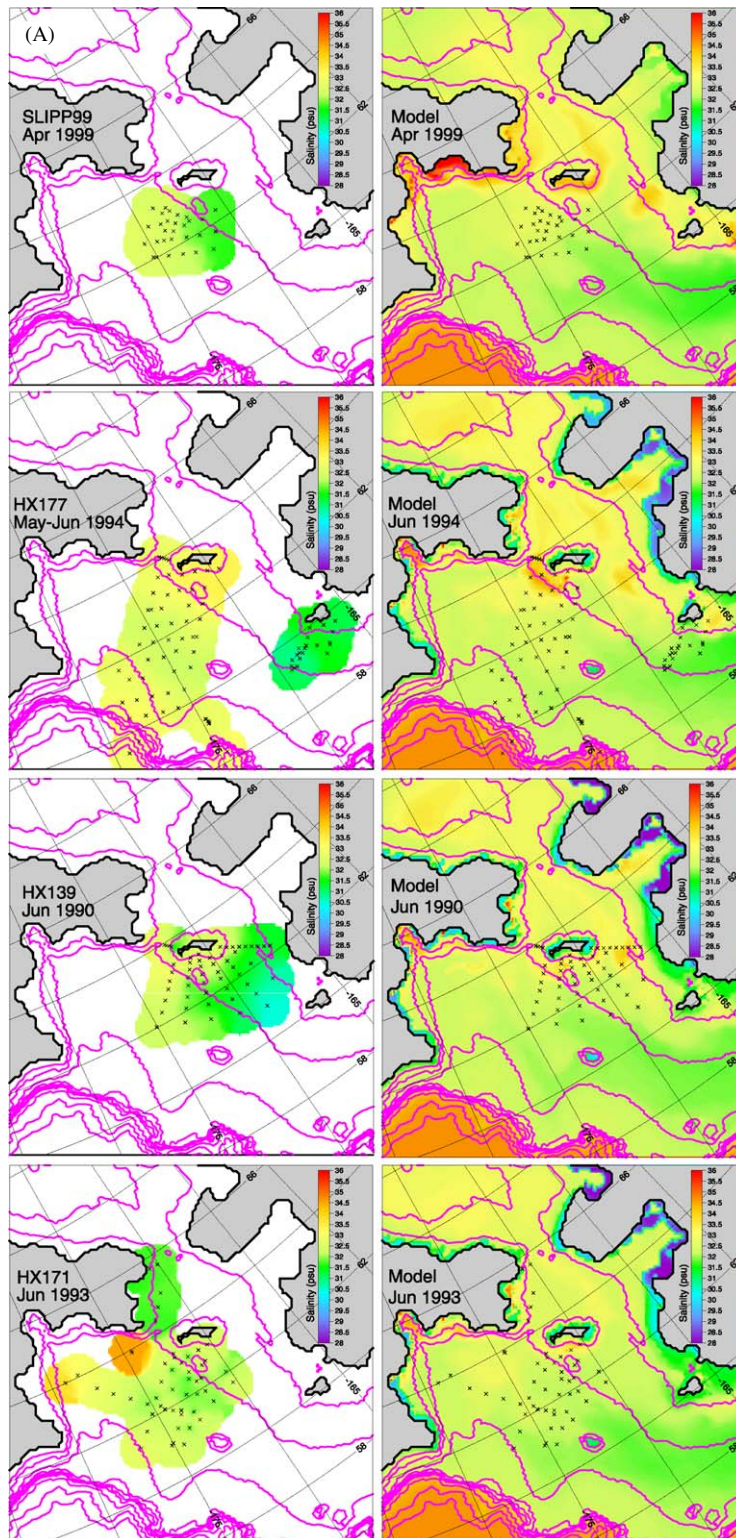


Fig. 20. Comparison of near bottom salinity between cruise observations (left) and model output (right): (A) during late winter through early summer, (B) during summer through early autumn.

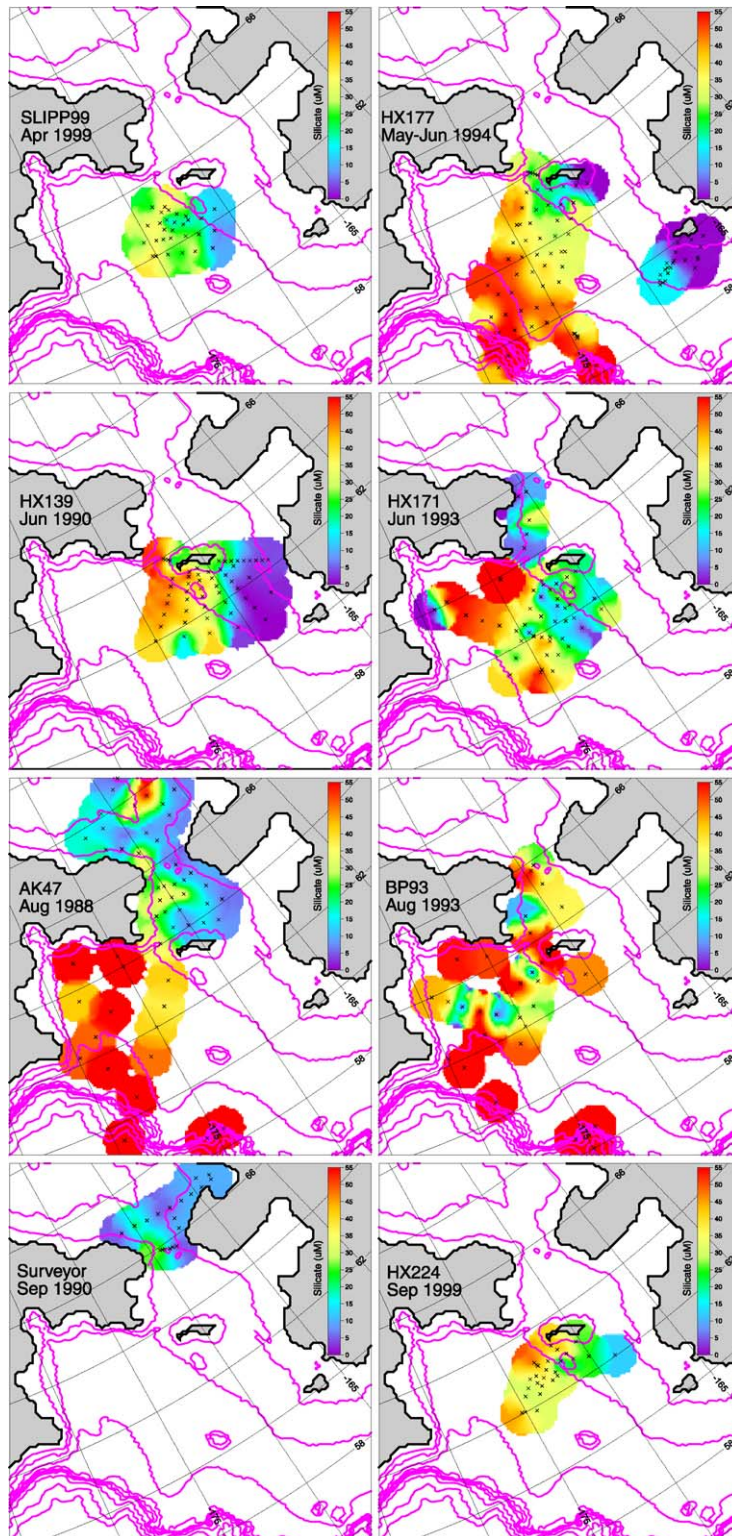


Fig. 21. Silicate concentration (μM) in near bottom samples collected during various cruises.

can be a proxy for silicate concentration in near-bottom waters of the Bering Sea. Therefore, regions of high salinity, which are just downstream from regions characterized by highly energetic mixing, may support higher primary production through vertical movement of nutrients into the euphotic zone. Specifically, these regions of known high primary and secondary (benthic) productivity, or 'hot spots', include the Chirikov Basin and the region just north of Bering Strait (Grebmeier et al., 1988; Springer and McRoy, 1993; and Grebmeier and Dunton, 2000). The high modeled EKE (Figs. 16–19) combined with high salinity derived from the nutrient-rich Anadyr Water (Fig. 20) allows for higher biological production in these areas. It can be inferred that improved model simulations of the distribution of ocean salinity and eddies (EKE) could provide useful information about biological 'hot spots' and other high productivity regions.

9. Discussion

Volume transport through Bering Strait is estimated to be 0.65 Sv over the 23-year simulation, while Roach et al. (1995) estimate approximately 0.83 Sv during October 1990–October 1994. When we compare model output for the same time interval, the model estimate is 0.58 Sv. The differences in these transport volumes may arise due to several factors. A possible source of discrepancy between observations and model results is the model atmospheric forcing fields, which are smoothed and of relatively low resolution, making the model less likely to simulate strong, local events. However, the observational estimates are based on point measurements and regressions with a short time-series of ADCP velocity measurements, while the model calculations integrate over horizontal and vertical axes and are numerically continuous in time. Both methods have associated errors, but the model results suggest that estimates of the Bering Strait transport derived from point observations are higher (~27%) than the estimates derived from a method which utilizes velocities across the entire strait. According to the long-term mean model output (Fig. 9A), near-bottom velocities in the eastern and western channels of the Bering Strait are the highest of any point across the strait. This provides a very reasonable explanation of why observational estimates based on velocity time series

at one or two near-bottom points generally give higher transport values.

The modeled freshwater flux through Bering Strait indicates a wide range of interannual variation (981–1955 km³ yr⁻¹) and this variation is strongly linked to the overall volume transport. This flux may be in some instances an underestimate if we take into account the higher salinity values from the model relative to observations. However, it might be quite realistic given the errors in volume flux estimates and high correlation between volume and freshwater fluxes. The northward heat transport is also interannually variable (1.29–4.28 TW); however, it is largely independent of volume transport. It is also worth pointing out limitations to the field observations when used for similar flux calculations. The observations are made intermittently at three near-bottom mooring locations in the Bering Strait region and then are extrapolated to represent the entire section, which according to our model results experiences significant, seasonally dependent, horizontal and vertical gradients of water properties and flow structure. Modulation and variation of the northward heat and freshwater fluxes has downstream implications for sea-ice cover, stratification and nutrient budgets in the Chukchi Sea and Arctic Ocean.

In quantifying the circulation and water mass properties of the northern Bering Sea, we have considered times scales from a few days to inter-annual and decadal. Model estimates of the annual cycle of Bering Strait transport are most similar to those based on geostrophic winds and wind forcing has been shown to be an important factor in Bering Sea circulation. Although the annual cycle is particularly important because of the high seasonality of flow through Bering Strait and the seasonally variable energy levels (EKE) across the shelf, model results indicate that short-term events, such as the flow reversal in winter 2000–2001, and interannual variability also have a strong impact on the ocean circulation, property distribution, and the overall operation of this system.

In order to determine the characteristics of water flowing through Bering Strait, it is important to consider upstream conditions. In the model we observe that water from Anadyr Strait contributes 80% of the mean flow (23-year mean = 0.52 Sv) into the Chukchi Sea. The wider, but shallower Shpanberg Strait contributes only 0.13 Sv or 20% of the mean flow through Bering Strait and is primarily made up of relatively sluggish Alaska Coastal Water

and Bering Shelf Water. It is worth noting that not all of the water flowing through Anadyr Strait is associated with the Anadyr Current. Instead some water moving northward on the northern Bering shelf also can go west around St. Lawrence Island through Anadyr Strait to reach Bering Strait.

Since the majority of Bering Strait throughflow is associated with the Anadyr Current, it is important to observe the characteristics of this water. However, most of Anadyr Strait lies in Russian territorial waters and international research efforts have been significantly limited in this area. Additional scientific efforts and field observations including long-term moorings in the Gulf of Anadyr and on the western side of Bering Strait, would be critical for determining the characteristics of the Pacific inflow into the Chirikov Basin north of St. Lawrence Island and eventually into the Arctic Ocean through the Bering Strait. Such data would allow further validation and constraining of ocean models for climate study.

Modeled temperature shows an east–west gradient across the northern Bering shelf, similar to observations (e.g., Coachman, 1987; Grebmeier et al., 1988), due to the presence of warm Alaska Coastal Water to the east and cold Anadyr Water to the west. We also show a smaller north–south gradient in the 23-year mean surface water temperature, with slightly lower temperatures in Bering Strait as compared to Anadyr Strait. This cooling north of St. Lawrence Island (SLI) may be due to several factors, such as the presence of winter polynyas and ice production north of SLI and in Norton Sound (Pease, 1980) and flow reversals in Bering Strait, especially during autumn.

Comparisons of modeled and observed salinities show that the model represents both the general east–west gradient and the seasonal changes associated with sea-ice formation and melt. Future model improvements will include more realistic representation of the salinity and temperature impacts from additional freshwater sources in the region. The ability to explicitly resolve the warm, fresh Alaska Coastal Current would enhance salinity representation from the Gulf of Alaska into the Bering Sea and further downstream in the Arctic Ocean. Modeled vertical sections across the two Pacific Water pathways toward Bering Strait show narrow coastal currents (< 30 km) and separation of flow. With the present model resolution (~9 km) such scales are not fully resolved. Higher resolution will also be critical for resolving eddies, which have

been demonstrated to be important for the circulation in the northern Bering Sea (Figs. 16–19). Also, tides are known to be important in many areas for ocean mixing and overall circulation. However, tides across the northern Bering shelf are much weaker compared to those over the southeast shelf and Aleutian Island regions (Kowalik, 1999) so their absence may not be highly detrimental to our overall model results. An exception would be the advection of mass and properties across the eastern Aleutian Island passes, which are known to be strongly affected by tides.

Because silicate concentrations can be estimated to some degree by salinity in sub-euphotic waters in the Bering Sea, this model has the potential to provide insights into the nutrient distribution across the shelf and through Bering Strait. This is especially important in regions that have been understudied, such as the Gulf of Anadyr and the western side of Bering Strait. Coincidentally, these same locations are thought to have high salinities and nutrient concentrations, which are important for biological production in the water column and the benthos. In addition, such information might be useful for the initialization and forcing of biological models using output from the physical model (e.g. Walsh et al., 2004).

10. Summary and conclusions

Mean velocity and total kinetic energy fields from our model generally show northward transport across the Bering Sea shelf with high velocity in narrow straits, such as Bering and Anadyr straits. Our analyses suggest that the method used to make observational estimates of volume transport through Bering Strait might overestimate the transport by as much as 27%. The importance of flow through Anadyr Strait is emphasized in its dominant contribution to Bering Strait throughflow and the similar seasonal and interannual patterns of water properties and flow observed in both Anadyr and Bering straits. Long-term measurements in that region would be critical for model validation and improvement. Time-series of volume transport show that the model is able to represent anomalous events, such as major flow reversals, which are corroborated by observations. Wind appears to be the dominant force driving water and ice movement across the northern Bering Sea at synoptic to interannual time scales. In addition to wind forcing, it is also important to consider buoyancy forcing

along the Alaska coast. Comparisons of modeled salinities with salinity observations show that the model is able to reproduce the characteristics of major water masses across the Bering shelf and in Bering Strait. However, incorporation of additional river sources and higher model resolution is needed, especially to improve representation of the lower salinity ranges in the Alaska Coastal Current along the southwestern Alaskan coast. EKE fields show that the NBS maintains year-round high energy and mixing, especially in Bering and Anadyr straits. Notably, these regions of high EKE are found just upstream of highly productive areas in the Bering Sea (e.g., the Chirikov Basin and the region just north of Bering Strait) that have been identified in previous studies such as Grebmeier et al. (1988), Springer and McRoy (1993), and Grebmeier and Dunton, (2000). This suggests that high-nutrient Anadyr Water is mixed into the euphotic zone as it flows generally northward and, upon encountering a region of lower EKE, can support water column primary production and the settling of organic matter to the benthos.

Acknowledgments

We thank the U.S. National Science Foundation/Shelf-Basin Interactions (SBI) Program for primary support of this research. Additional support has been provided through other National Science Foundation grants, the U.S. Department of Energy, and the National Oceanic and Atmospheric Administration. Computer resources were provided by the Arctic Region Supercomputing Center (ARSC) through the U.S. Department of Defense High Performance Computer Modernization Program (HPCMP) Grand Challenge Project. We thank Rodger Harvey, a guest editor of this volume, and two anonymous reviewers for constructive comments, which improved an earlier version of this manuscript.

References

- Aagaard, K., Carmack, E.C., 1989. The role of sea-ice and other fresh water in the Arctic circulation. *Journal of Geophysical Research* 94, 14485–14498.
- Aagaard, K., Roach, A.T., Schumacher, J.D., 1985. On the wind-driven variability of the flow through Bering Strait. *Journal of Geophysical Research* 90, 7213–7221.
- Clement, J.L., Cooper, L.W., Grebmeier, J.M., 2004. Late winter water column and sea-ice conditions in the northern Bering Sea. *Journal of Geophysical Research* 109 (C3), C03022.
- Coachman, L.K., 1987. Advection and mixing on the Bering–Chukchi Shelves. Component A. Advection and mixing of coastal water on high latitude shelves. ISHTAR 1986 Progress Report, vol. I, Institute of Marine Science, University of Alaska, Fairbanks, pp. 1–42.
- Coachman, L.K., 1993. On the flow field in the Chirikov Basin. *Continental Shelf Research* 13, 481–508.
- Coachman, L.K., Aagaard, K., 1988. Transports through Bering Strait: annual and interannual variability. *Journal of Geophysical Research* 93, 15535–15539.
- Cooper, L.W., Whitley, T.E., Grebmeier, J.M., Weingartner, T., 1997. The nutrient, salinity, and stable oxygen isotope composition of Bering and Chukchi seas waters in and near the Bering Strait. *Journal of Geophysical Research* 102, 12563–12573.
- Goosse, H., Campin, J.M., Fichefet, T., Deleersnijder, E., 1997. Sensitivity of a global ice–ocean model to the Bering Strait throughflow. *Climate Dynamics* 13 (5), 349–358.
- Grebmeier, J.M., Cooper, L.W., 1995. Influence of the St. Lawrence Island Polynya upon the Bering Sea benthos. *Journal of Geophysical Research* 100, 4439–4460.
- Grebmeier, J.M., Dunton, K.H., 2000. Benthic processes in the northern Bering/Chukchi seas: status and global change. In: Huntington, H.P. (Ed.), *Impacts of Changes in Sea-ice and Other Environmental Parameters in the Arctic*. Report of the Marine Mammal Commission Workshop, 15–17 February 2000, Girdwood, Alaska.
- Grebmeier, J.M., McRoy, C.P., Feder, H.M., 1988. Pelagic–benthic coupling on the shelf of the northern Bering and Chukchi seas. I. Food supply source and benthic biomass. *Marine Ecology Progress Series* 48, 57–67.
- Hermann, A.J., Stabeno, P.J., Haidvogel, D.B., Musgrave, D.L., 2002. A regional tidal/subtidal circulation model of the southeastern Bering Sea: development, sensitivity analyses and hindcasting. *Deep-Sea Research II* 49, 5945–5967.
- Jakobsson, M., Cherkis, N., Woodward, J., Macnab, R., Coakley, B., 2000. New grid of Arctic bathymetry aids scientists and mapmakers. *Eos Transactions AGU* 81 (9), 89.
- Kowalik, Z., 1999. Bering Sea Tides. In: Loughlin, T.R., Ohtani, K.O. (Eds.), *The Bering Sea: Physical, Chemical and Biological Dynamics*. Alaska Sea Grant Press, Fairbanks, AK, pp. 93–127.
- Maslowski, W., Walczowski, W., 2002. Circulation of the Baltic Sea and its connection to the Pan-Arctic region—a large scale and high-resolution modeling approach. *Boreal Environment Research* 7 (4), 319–325.
- Maslowski, W., Marble, D., Walczowski, W., Schauer, U., Clement, J.L., Semtner, A.J., 2004. On climatological mass, heat, and salt transports through the Barents Sea and Fram Strait from a pan-Arctic coupled ice-ocean model simulation. *Journal of Geophysical Research* 109, C03032.
- Muench, R.D., Ahlnäs, K., 1976. Ice movement and distribution in the Bering Sea from March to June 1974. *Journal of Geophysical Research* 81, 4467–4476.
- Nihoul, J.C.J., Adam, P., Bresseur, P., Deleersnijder, E., Djenidi, S., Haus, J., 1993. Three-dimensional general circulation model of the northern Bering Sea’s summer ecohydrodynamics. *Continental Shelf Research* 13, 509–542.
- Overland, J.E., 1981. Marine climatology of the Bering Sea. In: Hood, D.W., Calder, J.A. (Eds.), *The Eastern Bering Sea Shelf: Oceanography and Resources*, vol. 1. University of Washington Press, Seattle, pp. 15–22.

- Overland, J.E., Pease, C.H., 1982. Cyclone climatology of the Bering Sea and its relation to sea-ice extent. *Monthly Weather Review* 110, 5–13.
- Overland, J.E., Roach, A.T., 1987. Northward flow in the Bering and Chukchi seas. *Journal of Geophysical Research* 92, 7097–7105.
- Pease, C.H., 1980. Eastern Bering Sea-ice process. *Monthly Weather Review* 108, 2015–2023.
- Roach, A.T., Aagaard, K., Pease, C.H., Salo, S.A., Weingartner, T., Pavlov, V., Kulakov, M., 1995. Direct measurements of transport and water properties through the Bering Strait. *Journal of Geophysical Research* 100, 18443–18457.
- Royer, T.C., 1981. Baroclinic transport in the Gulf of Alaska, Part II. A fresh water driven Coastal Current. *Journal of Marine Research* 39, 251–266.
- Schumacher, J.D., Aagaard, K., Pease, C.H., Tripp, R.B., 1983. Effects of a shelf polynya on flow and water properties in the northern Bering Sea. *Journal of Geophysical Research* 88, 2723–2732.
- Spaulding, M., Isaji, T., Mendelsohn, D., Turner, A.C., 1987. Numerical simulation of wind-driven flow through the Bering Strait. *Journal of Physical Oceanography* 17, 1799–1816.
- Springer, A.M., McRoy, C.P., 1993. The paradox of pelagic food webs in the northern Bering Sea. III. Patterns of primary production. *Continental Shelf Research* 13, 575–599.
- Stabeno, P.J., Bond, N.A., Kachel, N.K., Salo, S.A., Schumacher, J.D., 2001. On the temporal variability of the physical environment over the southeastern Bering Sea. *Fisheries Oceanography* 10 (1), 81–98.
- Steele, M., Morley, R., Ermold, W., 2000. PHC: a global ocean hydrography with a high quality Arctic Ocean. *Journal of Climate* 14 (9), 2079–2087.
- Tsunogai, S., Kusakabe, M., Iizumi, H., Koike, I., Hattori, A., 1979. Hydrographic features of the deep water of the Bering Sea—the sea of silica. *Deep-Sea Research* 26A, 641–659.
- Walsh, J.J., Dieterle, D.A., Maslowski, W., Whittedge, T.E., 2004. Decadal shifts in biophysical forcing of Arctic marine food webs: numerical consequences. *Journal of Geophysical Research* 109, C05031.
- Walsh, J.J., McRoy, C.P., Coachman, L.K., Goering, J.J., Nihoul, J.J., Whittedge, T.E., Blackburn, T.H., Parker, P.L., Wirick, C.D., Shuert, P.G., Grebmeier, J.M., Springer, A.M., Tripp, R.D., Hansell, D.A., Djenidi, S., Deleersnijder, E., Henriksen, K., Lund, B.A., Andersen, P., Müller-Karger, F.E., Dean, K., 1989. Carbon and nitrogen cycling within the Bering/Chukchi Seas: source regions for organic matter effecting AOU demands of the Arctic Ocean. *Progress in Oceanography* 22, 277–359.
- Woodgate, R.A., Aagaard, K., Weingartner, T., 2005. Monthly temperature, salinity, and transport variability of the Bering Strait throughflow. *Geophysical Research Letters* 32 (4).